AMERICAN UNIVERSITY OF BEIRUT

REFLECTIVITY-BASED TECHNIQUE FOR THE DETERMINATION OF THE DIELECTRIC PROPERTIES OF MATERIALS: APPLICATION TO SILICON CARBIDE

by

TAMARA FADI AYACHE

A thesis
submitted in partial fulfillment of the requirements
for the degree of Master of Science
to the Department of Physics
of the Faculty of Arts and Sciences
at the American University of Beirut

Beirut, Lebanon
October 2014

AMERICAN UNIVERSITY OF BEIRUT

REFLECTIVITY-BASED TECHNIQUE FOR THE DETERMINATION OF THE DIELECTRIC PROPERTIES OF MATERIALS: APPLICATION TO SILICON CARBIDE

by

TAMARA FADI AYACHE

Approved by:

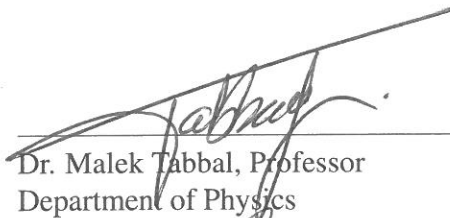

Dr. Malek Tabbal, Professor — Advisor
Department of Physics

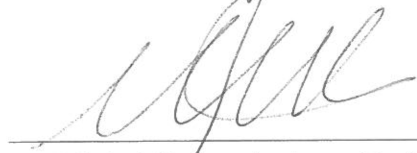

Dr. Michel Kazan, Assistant Professor — Committee Member
Department of Physics

Dr. Charbel Madi, Visiting Assistant Professor — Committee Member
Department of Physics

Date of thesis defense: October 14, 2014

AMERICAN UNIVERSITY OF BEIRUT

THESIS, DISSERTATION, PROJECT RELEASE FORM

Student Name:

Ayache	Tamara	Fadi
Last	First	Middle

● Master's Thesis ○ Master's Project ○ Doctoral Dissertation

☒ I authorize the American University of Beirut to: (a) reproduce hard or electronic copies of my thesis, dissertation, or project; (b) include such copies in the archives and digital repositories of the University; and (c) make freely available such copies to third parties for research or educational purposes.

☐ I authorize the American University of Beirut, **three years after the date of submitting my thesis, dissertation, or project,** to: (a) reproduce hard or electronic copies of it; (b) include such copies in the archives and digital repositories of the University; and (c) make freely available such copies to third parties for research or educational purposes.

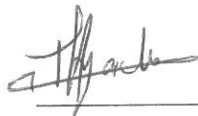

23/10/2014

Signature Date

This form is signed when submitting the thesis, dissertation, or project to the University Libraries

ACKNOWLEDGEMENTS

Above all, I thank God for letting me through all difficulties. He is the one who let me finish my bachelor's degree successfully, for without His guidance and blessings I would have done nothing.

It would not have been possibleto complete this thesis without the valuable contributions and support of my professors in AUB, to each of whom I owe my deepest gratitude.

In particular, I would like to express my sincere gratitude to my advisor Dr. Malek Tabbal for giving me the opportunity of working in the field of material physics as well as for his constant support and follow-up. I could not have imagined having a better advisor for my thesis study. I am as well grateful to Dr. Michel Kazan for his patience and willingness to back me up with his immense knowledge in the field. I am also thankful to Dr. Samih Isber, the chairperson of the physics department, for continually motivating and helping students throughout their years of study in AUB. Special thanks to Dr. Charbel Madi who agreed to be on my committee.

The SiC reflectivity measurements were performed at the Central Research Science laboratory (CRSL) at the American University of Beirut. Support by the CRSL crew especially Joan Younes and Rania Shatila is thankfully acknowledged.

I also wish to thank my friends who, not only made my stay in AUB a really enjoyable one, but who also lend me a hand especially Ali Abou Khalil who always offered to help me in working with the Latex program.

Last, but by no means least, I extend my thanks to my parents and family for raising me, supporting me, teaching me and loving me. To you I dedicate this thesis.

AN ABSTRACT OF THE THESIS OF

Tamara Fadi Ayache for Master of Science
Major: Physics

Title: Reflectivity-based technique for the determination of the dielectric properties of materials: application to Silicon Carbide

Silicon Carbide (SiC) is a group IV semiconductor material that can function under extreme conditions such as high-operating temperature, high power, high switching frequency and high breakdown voltage. The wide band gap of SiC (2.2-3.3 eV) is useful for realizing short wavelength blue and ultraviolet optoelectronic devices such as light-emitting diodes. For this reason, there is much interest in studying the optical properties of the SiC near its band gap edge. Many authors investigated the dielectric functions of the most common SiC polytypes (3C, 4H- and 6H-SiC) using spectroscopic ellipsometry for experimental studies and first-principles calculations in theoretical works. However, these latter techniques suffer from the drawback of having too many fitting parameters and the assumption of a defect free pure crystal, respectively. In this work, we are proposing a new technique to determine, without the use of any fitting parameters, the dielectric properties of 4H- and 6H-SiC around the band gap. We start by measuring the reflectivity spectra of 4H- and 6H-SiC, using the UV-VIS spectrophotometer, for angles of incidence,θ, ranging from 10 to 60°, using p and s polarized light. The experimental reflectivity values are used to obtain the frequency-dependent dielectric constant,ε , using the Kramers-Kronig equations, from which we extract the isotropic $\varepsilon_{\parallel}$, the index of refraction,n, and the extinction coefficient,k. We found that our real (imaginary) values for the dielectric constant ε are lower (higher) than those reported in the literature. This is explained by the fact that our technique takes into account the presence of defects in the lattice, which enhance the absorbance of the material. This work contributes to the understanding of the relation between the silicon carbide polymorphism and the optical properties of a realistic defect containing SiC lattice.

CONTENTS

Page

AKNOWLEDGEMENTS . . . . **v**

ABSTRACT . . . . **vi**

I. Introduction **1**

A. Silicon Carbide structure, bulk single crystal optical properties and applications 1

B. Structure of the thesis 5

II. Literature Review **6**

III. Experimental and numerical techniques **12**

A. Samples' Description 12

B. Ultraviolet Visible spectroscopy 13

1. Experimental setup 13
2. Operating Procedure 15

C. Overview on Maxwell's equations 16

D. Kramers-Kronig Method 18

1. Overview 18
2. Mathematical Derivations 19

E. Numerical determination of n and k 25

IV. Results and Discussion **27**

A. Reflectivity Measurement 27

1. p-polarized light 27
2. s-polarized light 30

B. Determination of n as a function of energy 32
1. p-polarized light 32
2. s-polarized light 34

C. Determination of k as a function of energy 35
1. p-polarized light 36
2. s-polarized light 37

D. Determination of the isotropic n and k 39
1. 4H-SiC 40
2. 6H-SiC 41

E. Comparison with literature 44
1. Dielectric function 44
2. Index of refraction 47

V. Conclusion and Future Work **49**

CHAPTER I

INTRODUCTION

A. Silicon Carbide structure, bulk single crystal optical properties and applications

Silicon Carbide (SiC) is a group IV compound semiconductor known for its ability to function under extreme conditions such as high-operating temperatures, high power, high switching frequency and high breakdown voltage [1]. There exists around 200 different polytypes of silicon carbide. Common to all these structures is the single basic unit that makes up the crystal, a layer of tetrahedra, where each silicon atom is tetrahedrally bonded to four carbon atoms and similarly each carbon atom is tetrahedrally bonded to four silicon atoms as shown in Figure 1. The length of the Si-C and Si-Si bonds is 0.422 * *a* and 0.707 * *a*, respectively, where *a* is the lattice constant of the crystal.

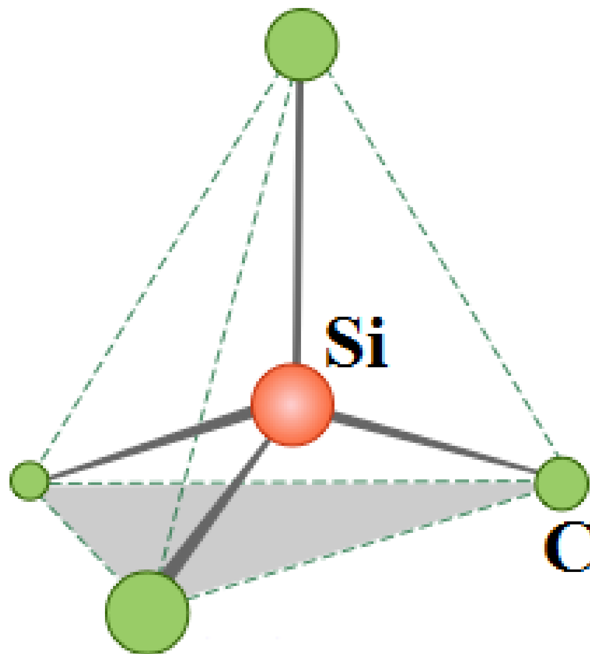

Figure 1: Tetrahedral coordination between Si and C atoms in SiC

What is different between these polytypes is the orientational sequence by which

each tetrahedral layer is stacked one on top of the other. The stacking of successive layers happens with many different sequential combinations that account for the different polytypes of SiC. A listing of the most common polytypes includes 3C, 2H, 4H, 6H, 8H, 9R, 10H, 14H, 15R,19R, 2OH, 21H, and 24R where (C), (H) and (R) refer to the three basic cubic, hexagonal and rhombohedral crystallographic categories respectively [1]. The most widely used polytypes are 3C-, 4H- and 6H-SiC. 4H- and 6H-SiC are a mixture of zinc-blende and wurtzite structure of SiC [2] with different stacking sequences as shown in Figure 2 :

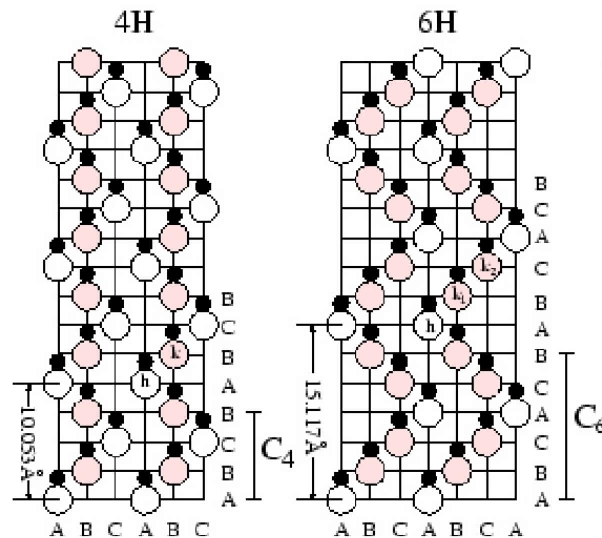

Figure 2: Arrangement of Si (open circles) and C (filled circles) atoms in the 4H- and 6H-SiC polytype (reproduced from [2])

The wurtzite ABCBA... stacking sequence is denoted as 4H-SiC reflecting its four bilayer stacking periodicity, while the stacking sequence of 6H-SiC is over 6 bilayers. They possess a hexagonal symmetry which makes them optically anisotropic uniaxial crystals. Table 1 shows some properties of the major polytypes of SiC: [3, 4, 5, 6, 7]

Table 1: Some properties of the 3C- 4H- and 6H-SiC at room temperature 300K

Polytype	3C-SiC (β-SiC)	4H-SiC (α-SiC)	6H-SiC (α-SiC)
Crystal structure	Zinc-blende (Cubic)	Hexagonal	Hexagonal
Lattice constant	a=4.3596	a=3.073	a=3.0806
		c=10.053	c=15.1173
Density (g/cm^3)	3.21	3.211	3.21
Bandgap (eV)	2.36	3.23	3.05
Bulk Modulus (GPa)	250	220	220
Saturated electron drift velocity($10^7 cms^{-1}$)	2.5	2	2
Thermal conductivity (W.$cm^{-1}.K^{-1}$)	3.2	3.7	3.6

SiC is an indirect bandgap semiconductor. G. Wellenhofer [8] presented the band structure of several polytypes of SiC, 2H-, 3C-, 4H-, 6H-, and 15R-SiC from ab-initio calculations. The intimate relation between the electronic and crystalline structures results in the modification of the electron band structure as the stacking sequence increases from 2H- to 15R-SiC.

With the increasing miniaturization of electronic circuits, SiC presents several advantages over Si. The room temperature bandgap energy of 3C-, 4H- and 6H-SiC is 2.3, 3.2, and 3.0 eV, respectively [6]. These are two to three times greater than the bandgap of Si (1.1 eV) [9]. This wide bandgap energy results in SiC maintaining its semiconductor behavior at high temperature more than Si does, due to its low intrinsic carrier concentration. This property allows building dynamic memories (DRAMs) in SiC.

The thermal conductivity of SiC is 3.2 W $cm^{-1}K^{-1}$ for 3C-SiC, 3.6 W $cm^{-1}K^{-1}$ for 6H-SiC and 3.7 W $cm^{-1}K^{-1}$ for 4H-SiC. These are also more than three times larger than that of Si. Therefore, SiC is an excellent thermal conductor which enables heat to flow through it more readily than other semiconductor materials. It is used as a themal

shock resistant material as well as to manufacture high power electronic devices [7].

SiC can tolerate high voltage gradients such as 2.2 $\times 10^6$ V/cm which is 5 times greater than what Si can endure (3×10^5 V/cm). This makes SiC one of the most suitable candidates for high power and high voltage devices such as field effect transistors, bipolar storage capacitor, ultraviolet detectors and thyristors [7].

At low electric fields, the drift velocity and **E** are linearly related by the proportionality constant μ :$v_d = \mu\mathbf{E}$. At high electric fields, this velocity is independent of impurity dopings and attains its highest value ranging from 2×10^7 cm/s for 4H- and 6H-SiC to 2.5×10^7 cm/s for 3C-SiC which is much larger than Si and GaAs. This property enables SiC to operate in high frequency devices at radio and microwave frequencies [7].

Besides its optical, thermal and electrical properties, SiC is well known for being mechanically hard, chemically inert and very stable at temperatures above 300°C. These characteristics rank SiC as number one in the fabrication of MEMS(integrated microdevices) whose applications include accelerometers, pressure, chemical and flow sensors as well as in the building of resistance heating elements for electric furnace and fundamental constituents for thermistors and varistors [7].

Besides the electrical and mechanical properties, it is essential to know the optical constants n and k of SiC polytypes because of their contribution to optoelectronic device design. The wide band gap of SiC is useful for realizing short wavelength blue and ultraviolet optoelectronics. SiC-based blue pn junction light emitting diodes LEDs were the first silicon carbide based devices to reach high volume commercial sales. These diodes were the first mass-produced LEDs to cover the blue (250 to 280 nm peak wavelength) portion of the visible color spectrum, which in turn enabled the realization of the first viable full-color LED-based displays. In addition, the optical properties of SiC will serve as a reference point to the material's quality and control during production [10]. However, the enhancement of the performance of such optoelectronic devices requires that the band gap bulk dielectric properties of the SiC polytypes be known as precisely as possible. From here stems our interest to compute the dielectric function, ordinary

and extraordinary index of refraction, n, as well as extinction coefficient, k, around the bandgap of SiC.

B. Structure of the thesis

The structure of the thesis is outlined as follows: after introducing the properties and applications of SiC in this first chapter, we will examine the optical studies done on SiC by different authors in the second chapter. The third chapter will present the experimental aspects of the work, explain Kramers-Kronig Method (K-K method) and our new numerical technique to extract the optical properties of our samples namely bulk 4H- and 6H-SiC. In the fourth chapter, we will present the experimental results and their analysis leading to the determination of n and k near the bandgap edge. We will conclude in the final chapter and present perspectives for future work.

CHAPTER II

LITERATURE REVIEW

In this chapter, we will present a survey of the literature on optical studies completed on SiC.

Several works were done to investigate the reflectivity studies on cubic and wurtzite-structure of SiC crystal. One of the earliest works is the normal incidence ultraviolet reflection spectra of 6H, 15R and β-SiC reported by B.E. Wheeler [11]. Gavrilenko [12] evaluated the electroreflection spectra of 4H- and 6H-SiC in the energy range of 1.0 and 5.6 eV by using the multiple-oscillator model. We also mention the work of Lambrecht [13] who found the experimental and theoretical optical reflectivity in the range of 4-10 eV of 3C and 4H polytypes of SiC using the linear muffin-tin orbital method (LMTO) and the local density approximation. Theoretical calculations (from LMTO) and measured UV-reflectivity agree except for a bandgap shift of a 1 eV. The same group [14] extended their study to predict systematically the vacuum uv-reflectivity for $\mathbf{E} \perp$ to the c-axis of the SiC polytypes in the energy range of 4 to 10 eV. Experimental results of 4H-, 15R-, 6H-, and 3C-SiC were compared to the theoretical ones and good agreement was found.

Further experimental studies were to be performed to determine the dielectric function of SiC polytypes. To start with, Kildemo and colleagues [15] inspected the optical properties of the lightly doped 4H, 6H, 15R, and 21R-SiC polytype. The ordinary component of the dielectric function was determined from phase modulated spectroscopic ellipsometry (PMSE) and the extraordinary component is deduced from Kramers-Kronig (K-K) method. It was found that the dielectric difference function strength varies as a

cubic degree polynomial and that its turning point occurs at 50 % of its hexagonality. Conventional and synchrotron-radiation spectroscopic ellipsometry were used by Logothetidis and Petalas [10] to measure the perpendicular component of the dielectric function, the reflectivity spectrum and the dispersion of the index of refraction of 3C-SiC and bulk 6H-SiC in the energy region of 1.5 to 9.5 eV. The difference in the dielectric function curves of the two polytypes (3C- and 6H-SiC) accounts for the different crystal symmetry of the samples. Nonetheless, they maintain a similar broadening form for energies between 6.5 and 9 eV. For both polytypes, maxima in reflectivity occur at the same energy 7.8 eV. The index of refraction of 3C-SiC was determined from 1.5 to 5.5 eV. The study that made use of the Sellmeir Model extended the measurements done by Schaffer [16] in 1971 over the energy interval from 1.77 to 2.76 eV.

Spectroscopic rotating-analyzer ellipsometry was used by Zollner and co-workers [17] to measure the parallel component of the dielectric function of bulk 4H- and 6H-SiC in the energy range from 0.72 to 6.6 eV. Low energy and high energy values were fitted using single Lorentz Oscillator and Sellmeir Model equation, respectively. The authors noted that the surface roughness and the oxide overlayer affect the real as well as the imaginary components of ε especially at an energy beyond 5 eV. After correcting for the oxide layer, they concluded that ε_1 and ε_2 differ from previous results for energies between 4 and 6 eV while being similar for energies below 4 eV. Comparison with the work of Logothetidis [10] shows that the latter witnesses a zero value of ε_2 for 3C- and 6H-SiC at energies below the gap which is attributed to the incorrectness of the oxide layer.

Cobet and his partners [18] also used spectroscopic ellipsometry in order to obtain the ordinary dielectric function of 3C-,4H- and 6H-SiC from 3.5 to 10 eV, by allowing for surface roughness data correction with a three-phase model. Lindquist and his col-

leagues [19] investigated both the ordinary and extraordinary dielectric function of 4H- and 6H-SiC from 3.5 to 9 eV using ultraviolet spectroscopic ellipsometry (UVSE). Similarly to Zollner's work [17], they mathematically corrected the SiO_2 layer which should be considered in the model to improve accuracy in spectral peak positions and amplitudes. Agreement between ab-initio and this method is pointed out at the level of simple trends. Effects of polytypism in the dielectric constants is more highlighted in $\varepsilon_{||}$ than in $\varepsilon_{\perp}$ since the stacking sequence of Si and C layers are different in the direction parallel to the c-axis. These experimental results confirm the high anisotropy of SiC polytypes in the UV region of ε as anticipated by theory.

Combining experimental and theoretical techniques in one paper, Ahuja and coworkers [20] investigated the bandgap energy and dielectric function of n-doped 4H-SiC experimentally by transmission spectroscopy and spectroscopic ellipsometry and theoretically by an ab initio full-potential linear muffin-tin-orbital method. Agreement between the two methods is attained after the correction of the bandgap which shifts the calculated ε_2 upwards in photon energy. The fact that the real component of dielectric function differ in the longitudinal and transverse directions concludes that the anisotropy of 4H-SiC is small.

Studies based solely on theoretical models include that of Changkun [21] who examines the graphs of the longitudinal and transverse components of real and imaginary parts of ε of 6H-SiC using ab initio methods. The imaginary part is obtained directly using joint Density Of States (DOS) and the real part is extracted from Kramers-Kronig relationship. Similar to Ahuja [20], a constant potential is applied to the conduction band state in order to correct the indirect bandgap. Agreement can be observed between this and the experimental work of Lindquist [19]. The calculated real and imaginary parts of the dielectric function allow the calculation of important optical constants such as the

reflectivity at normal incidence. In general, the calculated reflectivity spectra R is in agreement with the experimental work of Logothetidis [10].

B. Adolph and coworkers [22] performed similar measurements calculating the frequency dependent dielectric function of 2H-, 4H- and 6H-SiC as well as the cubic 3C-SiC by the ab initio pseudopotential-plane-wave method and random-phase approximation. Similar to Lindquist's findings [19], the graphs of the real and imaginary parts of the dielectric function show that the parallel component is more affected by the polytypism than the perpendicular one. The reflectivity spectra could be extracted from the real and imaginary parts of epsilon using fresnel's equation for normal incidence, assuming either a parallel or a perpendicular orientation to the optical axis. Intensity of reflectivity difference between their measurements and experimental results can be traced back to the overestimation of the high frequency dielectric constant and the non-broadening effect of theoretical models. The prediction of the frequency dependence of the real index of refraction n is provided for light polarized parallel and perpendicular to the c-axis. He concludes, in the wide wavelength range, that light polarized parallel to the c axis is more refracted than when it is perpendicularly polarized.

Susumu and Sadao [23] determined the optical constants of 6H-SiC using spectroscopic ellipsometry (SE) in the energy range of 1.2 to 5.4 eV. He obtained the complex dielectric function for light polarized parallel and perpendicular to the c-axis which was then analyzed using the Lorentz type model. The index of refraction of 6H-SiC, evaluated (for E$\leq$4.5 eV) using the first-order Sellmeier equation, contributed to the determination of high-frequency dielectric function for both polarizations which was found to agree with previous literature values. In addition, the authors computed the refractive index anisotropy $\Delta n = n_{\parallel} - n_{\perp}$ which showed to increase with increasing energy, and approximated the relation between Δn and E by a second degree polynomial.

M. Kildemo et al. [24] used phase-modulated spectroscopic ellipsometry (SE), polarised light transmission measurements and crossed polariser variable angle of incidence interferometry to find the uniaxial dielectric function of bulk semi-insulating 4H-SiC and doped 6H-SiC below and around the minimum band gap. They extracted the ordinary and extraordinary components of the dielectric constant by fitting a Sellmeier model. The resulting dielectric difference from the variable angle of incidence SE measurement shows that the absorption band will change the birefringence. Hence they deduced a relationship connecting the hexagonality of the SiC polytype to the "birefringence strength" of the dielectric difference.

Bechstedt et al. [25] applied the first-principles method (FPM) to compute the dielectric function of 3C-, 4H- and 6H-SiC. First-principles molecular dynamics (FPMD) was used by Yang and co-workers [26] to examine the optical properties of bulk 3C- and 6H-SiC in the energy range, 3-8 eV, including the temperature effect on optical properties of solids. With thermally equilibrated configuration and temperature modified electronic band structure, they calculated the finite temperature imaginary part of the dielectric function using the Fermi's Golden rule. The real part of the dielectric function is easily extracted from Kramers-Kronig dispersion relations. After presenting their calculated values of ε and the experimental results from other references [10, 17], Yang et al. noticed a slight difference due to the different conditions under which samples of SiC were synthesized. They concluded that the temperature modification on dielectric spectra is intrinsically related to the temperature disturbed electronic band structure and density of states.

Our observation from all of the above mentioned work is that the band gap dielectric properties of 4H- and 6H-SiC reported in the literature were deduced either by fit-

ting ellipsometry data using simplified physical models involving several free adjustable parameters or directly from first principles calculations, with variable agreement among authors. The analysis of optical spectra by well-established physical models has demonstrated high potential for everyday application for rough estimation of the dielectric properties in semiconductor materials. Nevertheless, such an approach becomes questionable when precise data are needed for very specific applications. On the other hand, the use of first principles calculations for data regarding the material dielectric properties is applicable only for highly purified materials in which the phonons and electrons transitions are the only determinants of the material dielectric properties with little contribution from defects. In the case where a convolution between the material intrinsic response and defects response is needed, such an approach becomes inappropriate. Therefore, a new method free of any adjustable parameters is required to provide reliable data concerning the dielectric function of materials that cannot be grown with a purity close to that of Silicon.

Among the optical measurement techniques, reflectivity spectroscopy remains the most quantitative one because the light reflectivity from a flat semiconductor surface can be described by simple theories and the reflectivity data can be converted to frequency-dependent dielectric through numerical or mathematical conversion such as the well-known Kramers-Kronig integral. In this thesis, we will use the UV (ultra violet)-VIS (visible)-NIR (near infrared) spectrophotometer to perform reflection measurements on bulk 4H-SiC and 6H-SiC, at different angles of incidence (0 to 60 degrees). Next, we will use the Kramers-Kronig method to extract the parallel and perpendicular components of the real and imaginary parts of ε. Then, we will make use of our newly developed technique, fully elaborated in chapter 3, to get the isotropic dielectric function as well as the index of refraction and extinction coefficient around the bandgap energy. This will contribute to the understanding of the relation between silicon carbide polymorphism and optical properties.

CHAPTER III

EXPERIMENTAL AND NUMERICAL TECHNIQUES

In this chapter, we will give a detailed account of the experimental aspects of the work as well as the analysis of the optical data. First, we will describe the way the 4H- and 6H-SiC samples were grown, and the UV-VIS spectrophotometer used for the reflection measurements. We also give a brief review on Maxwell's equations and the Kramers-Kronig method that allows the determination of the real and imaginary dielectric function for each frequency. The chapter concludes with a detailed description of our new technique that is a combination of Maxwell's equations and the Kramers-Kronig method, leading to the determination of the optical properties of the samples.

A. Samples' Description

The samples were grown by physical vapor transport (PVT) in the Department of Materials Science at the University of Erlangen, Germany by Prof. Boris Epelbaum's group [27]. In this technique, a solid source of SiC (powder or bulk SiC) is heated to a temperature high enough to induce evaporation of the SiC source, typically above 2000°C. The evaporation process takes place in vacuum or in an inert gas and the evaporated species re-condense on a seed SiC monocrystal that is kept at a lower temperature. This "seeded" PVT technique is the most suitable way to produce high quality single crystal SiC at a large scale [28]. For this work, the growth runs were performed in an inductively heated reactor at a pressure of 15-30 mbar (1500-3000 Pa) in pure Argon (Ar), on rhombohedral ($0\ 1\ \bar{1}\ n$) plane seeds, which were cut from standard (0 0 0 1) bulk 4H- and 6H-SiC crystals. 6H-SiC samples were grown at temperatures ranging from 2150 to 2250°C whereas the 4H-SiC samples were grown between 2100 and 2150°C. In both

cases, high quality micropipe-free (0 0 0 1) SiC crystals were obtained, as detailed in [27].

B. Ultraviolet Visible spectroscopy

1. Experimental setup

All our optical measurements were performed using a double beam V-570 UV-VIS spectrophotometer manufactured by JASCO corporation (Japan). Its optical system is shown in Figure 3:

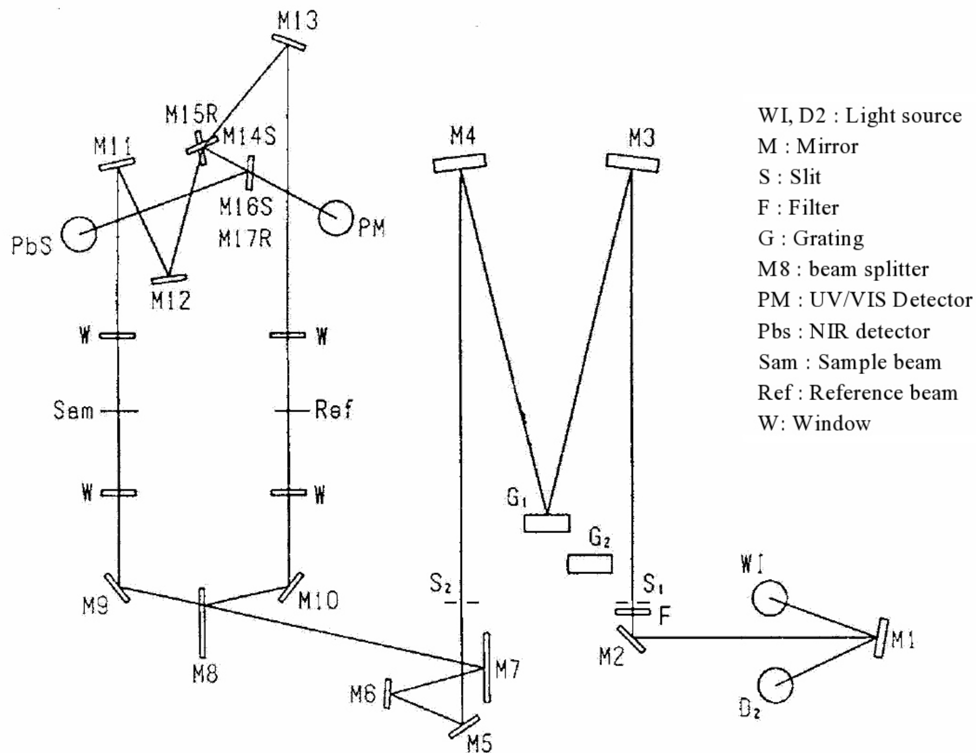

Figure 3: V-570 optical system

The V-570 can emit light in the range from 190 to 2500 nm. The light sources used are a deuterium (D2) lamp (190 to 350 nm) for use in the ultraviolet region and Halogen (WI) lamp (340 to 2500 nm) for use in the VIS/NIR region. The light from the source enters the monochromator and is dispersed by a grating in order to generate a

monochromatic light. The light is split into two beams using a beam-splitter: one incident on the actual sample and the other on the reference sample. The light that has passed through the sample and reference sample is incident on the photomultiplier tube or PbS photoconductive cell to detect the difference in signal between the two beams.

In this work, since we are performing reflectance rather than absorbance measurements, we attached the Absolute Reflectance Measuring Unit (ARMU) model shown in Figure 4 with its components in Figure 5:

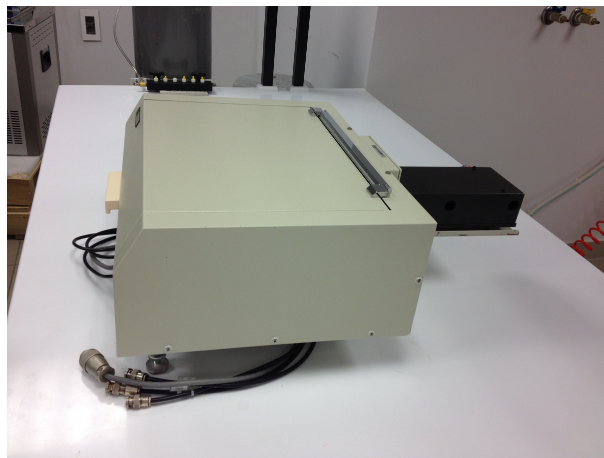

Figure 4: Absolute Reflectance Measuring Unit

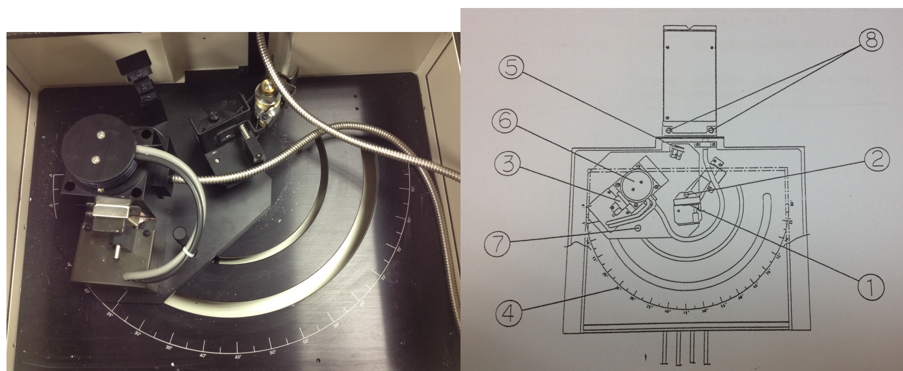

Figure 5: The components of ARV-474/ARV-475

The components of the ARMU are:

(1) The absolute reflectance measurement holder where the sample is mounted.

(2) Holder setscrew

(3) Relative reflectance measurement holder: used for relative measurements.

(4) Incident angle scale: Indicates the angle of incidence with respect to the sample for absolute reflectance measurements.

(5) Mirror: directs light into the integrating sphere.

(6) Integrating sphere: Model ARV-474 is equipped with a photomultiplier tube (PM) and Model ARN-475 with PM and Pbs photoconductive cell.

(7) Integrating sphere setscrew

(8) ARV-474/ARV-475 set-screw

2. Operating Procedure

This subsection describes the operating procedure for the Model ARV-474/ARV-475 to measure sample reflectance.

(1) Start the spectrophotometer.

(2) Dismount the standard absorbance unit and gently mount the absolute reflectance measuring unit (ARMU) in the sample chamber.

(3) Mount the standard reflection plate (white plate) on the relative reflectance measurement holder located on the rear of the integrating sphere.

(4) Remove the setscrew on the absolute reflectance measurement holder to dismount it.

(5) Set the integrating sphere at an incidence angle of 90° and fix it using the setscrew.

(6) Set spectrum measuring conditions and measure baseline correction data. This way we will insure that the line is within 100±1%R.

(7) Mount sample on the absolute reflectance measurement holder. (8) Mount the holder in position and fix it using setscrew. (9) Insert the polarizer(first p- then s-polarizer).

(10) Turn the integrating sphere to set the angle of incidence (to 5 then 10, 15,... 60°) and fix it using the setscrew.

(11) Press the start button to take measurement.(Set the photometric mode at %R)

(12) Save the reflectance graphs from the computer.

(13) Dismount the sample from the ARV-474/ARV-475.

C. Overview on Maxwell's equations

To study the reflectivity of a bulk crystal, it is essential to understand quantitatively the relationship between incident, reflected and transmitted amplitudes of the beam of light. For this reason, we use the electromagnetic theory by setting up Maxwell's equations and applying boundary conditions at the interface [29]. We start by assuming incident monochromatic light which forms plane waves with well defined k-vectors as shown in Figure 6:

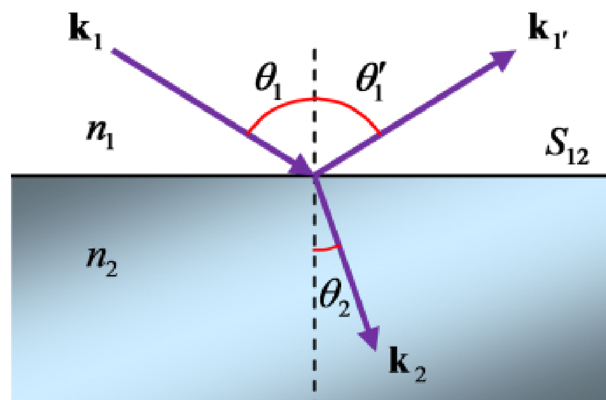

Figure 6: Electromagnetic approach at a surface

We will consider two polarizations of the electric field shown in Figure 7: A perpendicular "S" polarization where **E** is $\perp$ to the plane of incidence and a parallel "P" polarization where **E** is in the plane of incidence.

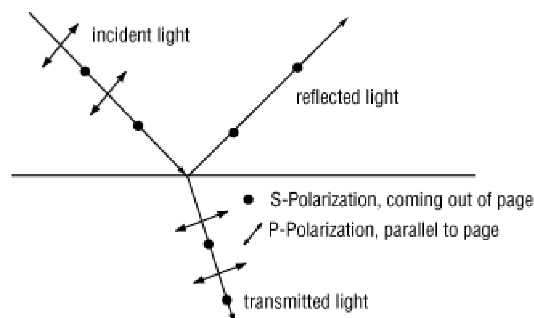

Figure 7: Electromagnetic approach at the surface

In regions of space where there is no free charge distributions and no free cur-

rents, Maxwell's equations for the electric and magnetic fields reduce to:

$$\begin{aligned}
\nabla.E &= 0 \\
\nabla.B &= 0 \\
\nabla \times E &= -\tfrac{\partial B}{\partial t} \\
\nabla \times B &= \mu\varepsilon\tfrac{\partial E}{\partial t}
\end{aligned} \tag{1}$$

where μ is the magnetic permeability, and ε is the dielectric permittivity. The above last two equations can be put into a well known simple form of wave equation:

$$c^2.\nabla^2.E = \mu\varepsilon\frac{\partial^2 E}{\partial^2 t} \tag{2}$$

$$c^2.\nabla^2.B = \mu\varepsilon\frac{\partial^2 B}{\partial^2 t} \tag{3}$$

where c is the speed of light. Equations (2) and (3) are under the form of

$$\nabla^2.E = \frac{1}{v^2}\frac{\partial^2 E}{\partial^2 t} \tag{4}$$

which by comparison shows that the velocity of the disturbances is expressed as :

$$v = \frac{c}{\sqrt{\mu\varepsilon}} \tag{5}$$

And we know from the definition of the index of refraction of a medium that $n = \sqrt{\mu\varepsilon}$ $\Longrightarrow\ v = \frac{c}{n}$. To describe the propagation of light in an absorbing medium, the refractive index n is replaced by a complex quantity

$$\tilde{n} = n + ik \tag{6}$$

where the real part n is the index of refraction and the imaginary part k is the absorption

coefficient. The dielectric function is expressed as

$$\tilde{\varepsilon} = \varepsilon_1 + i\varepsilon_2 \tag{7}$$

$\tilde{n}$ satisfies the relation

$$\tilde{n(\omega)} = \sqrt{\varepsilon(\omega)} \tag{8}$$

Since $\varepsilon(\omega)$ depends on the frequency ω, $\tilde{n}$ which is the square root of the epsilon function also depends on ω. From equation (8):

$$\varepsilon(\omega) = \tilde{n}^2 \tag{9}$$

If we expand (9), we will be able to relate the imaginary and real parts of ε and $\tilde{n}$ [30]:

$$\begin{cases} \varepsilon_1(\omega) &= n^2 - k^2 \\ \varepsilon_2(\omega) &= 2nk \end{cases} \tag{10}$$

and

$$\begin{cases} n &= \frac{1}{\sqrt{2}}\sqrt{\varepsilon_1(\omega) + \mid \varepsilon(\omega) \mid} \\ k &= \frac{1}{\sqrt{2}}\sqrt{-\varepsilon_1(\omega) + \mid \varepsilon(\omega) \mid} \end{cases} \tag{11}$$

where $\mid \varepsilon(\omega) \mid$ is the magnitude of $\varepsilon(\omega)$.

So now if we have ε_1 and ε_2, we can find from equations (11) n and k which are dependent on the frequency. In this way, the optical properties of the material can be revealed.

D. Kramers-Kronig Method

1. Overview

Many analytic complex functions have been developed in order to relate the real part of that function to an integral containing the imaginary part, and vice versa. The

Kramers-Kronig method, named after Ralph Kronig and Hendrik Anthony Kramers, is used to study this relation between the real and imaginary parts of response functions in physical systems. It can be applied to study complex optical functions describing light-matter interaction phenomena, such as susceptibility, the dielectric function, the index of refraction, and reflectivity. The Kramers-Kronig (K-K) relations are used in reflection spectroscopy to describe the relation between the measured reflectance and the phase of the reflectivity [31]. For the K-K relations to be applied, the complex response function $f(\omega) = f_1(\omega) + if_2(\omega)$ must satisfy the following conditions:

1. $f(\omega)$ must be analytic in the upper half of the complex plane, and the poles are below the real axis.

2. The real part $f_1(\omega)$ must be an even function and the imaginary part $f_2(\omega)$ must be odd for real values of ω.

3. The function must vanish at very high frequencies, i.e. the integral of $\frac{f(\omega)}{\omega}$ along a semicircle with infinite radius in the upper half of the complex plane vanishes.

Satisfying these conditions and using the Cauchy residue theorem for complex contour integration, the K-K relations are obtained.

2. Mathematical Derivations

Consider the function $\frac{f(s)}{s-\omega}ds$. This function is analytic in the upper half of the complex plane. By complex analysis, the residue theorem implies that the integral of this function on a closed contour defined by Figure 8 is zero.

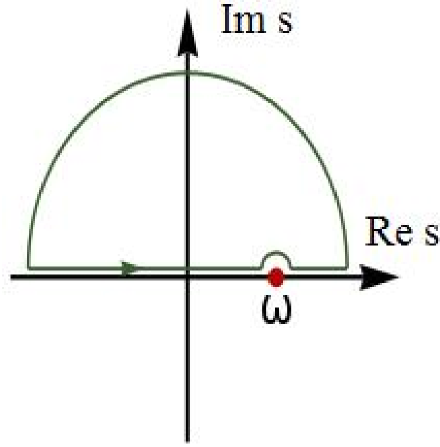

Figure 8: Contour used for deriving the Kramers-Kronig relations

The integral can now be separated into three regions. The first is along the big semicircle which turns out to be equal to zero by the residue theorem. The second region is along the real axis which is given by:

$$P\int_{-\infty}^{\infty}\frac{f(s)}{s-\omega}ds$$

where P is referred to the principle part of the integral.
And the third region is along the small semicircle at the pole s = ω which is given by - $i\pi f(\omega)$. This results in the following expression for the integral:

$$\int\frac{f(s)}{s-\omega}ds = P\int_{-\infty}^{\infty}\frac{f(s)}{s-\omega}ds - i\pi f(\omega) = 0 \tag{12}$$

Therefore, the expression of $f(\omega)$ is given by:

$$f(\omega) = \frac{1}{i\pi}P\int_{-\infty}^{\infty}\frac{f(s)}{s-\omega}ds \tag{13}$$

which is the compact form of Kramers-Kronig relations.
Consider a complex function: $\alpha(\omega) = \alpha_1(\omega) + i\alpha_2(\omega)$.
This function $\alpha(\omega)$ satisfies the conditions necessary for K-K relations. Therefore, it can

be written as:

$$\alpha = \frac{1}{i\pi} P \int_{-\infty}^{\infty} \frac{\alpha(s)}{s-\omega} ds$$

The function $\alpha(s)$ is also a complex function which takes the form: $\alpha(s) = \alpha_1(s) + i\alpha_2(s)$
Therefore, our equation becomes:

$$\alpha_1(\omega) + i\alpha_2(\omega) = \frac{1}{i\pi} P \int_{-\infty}^{\infty} \frac{\alpha_1(s) + i\alpha_2(s)}{s-\omega} ds$$

$$\implies \alpha_1(\omega) + i\alpha_2(\omega) = \frac{-iP}{\pi} \int_{-\infty}^{\infty} \frac{\alpha_1(s)}{s-\omega} ds + \frac{P}{\pi} \int_{-\infty}^{\infty} \frac{\alpha_2(s)}{s-\omega} ds$$

Taking the real part of each side we get:

$$\alpha_1(\omega) = \frac{P}{\pi} \int_{-\infty}^{\infty} \frac{\alpha_2(s)}{s-\omega} ds$$

Splitting the integral into two parts:

$$\alpha_1(\omega) = \frac{P}{\pi} \int_{-\infty}^{0} \frac{\alpha_2(s)}{s-\omega} ds + \frac{P}{\pi} \int_{0}^{\infty} \frac{\alpha_2(s)}{s-\omega} ds$$

Flipping the first integral and replacing s by -s:

$$\alpha_1(\omega) = \frac{P}{\pi} \left(\int_{0}^{\infty} \frac{\alpha_2(s)}{s+\omega} ds + \int_{0}^{\infty} \frac{\alpha_2(s)}{s-\omega} ds \right)$$

where we have used the second condition that α_2 must be odd: $\alpha_2(-s) = -\alpha_2(s)$

Doing common denominator :

$$\implies \alpha_1(\omega) = \frac{P}{\pi}\left(\int_0^\infty \frac{\alpha_2(s).(s-\omega)+\alpha_2(s).(s+\omega)}{(s-\omega)(s+\omega)}ds\right)$$

$$\implies \alpha_1(\omega) = \frac{P}{\pi}\left(\int_0^\infty \frac{\alpha_2(s).2s}{s^2-w^2}ds\right)$$

which finally gives the first relation of Kramers-Kronig:

$$\alpha_1(\omega) = \frac{2.P}{\pi}\int_0^\infty \frac{s.\alpha_2(s)}{s^2-w^2}ds \tag{14}$$

By similarly taking the imaginary part of each side we get:

$$\alpha_2(\omega) = \frac{-P}{\pi}\int_{-\infty}^\infty \frac{\alpha_1(s)}{s-\omega}ds$$

Splitting the integral into two parts, and using the second condition that α_1 must be even: $\alpha_1(-s) = \alpha_1(s)$, we get:

$$\alpha_2(\omega) = \frac{-P}{\pi}\left(\int_0^\infty \frac{-\alpha_1(s)}{s+\omega} + \int_0^\infty \frac{\alpha_1(s)}{s-\omega}ds]\right)$$

Which results in the second relation of Kramers-Kronig:

$$\alpha_2(\omega) = \frac{-2.\omega.P}{\pi}\int_0^\infty \frac{\alpha_1(s)}{s^2-\omega^2}ds \tag{15}$$

Using the K-K relations to analyse our reflectance data, we must be able to relate the amplitude of the reflectance to the phase change between the incident and reflected signal.

We first start with the relations:

$$R(\omega) = r(\omega)r^*(\omega) = \rho^2(\omega)$$

$$r(\omega) = \frac{E_{reflected}}{E_{incident}} = \rho(\omega)\exp(i\phi(\omega))$$

where R is the reflectivity, $r(\omega)$ is the Fresnel coefficient of reflectivity, $\rho(\omega)$ is the amplitude, and $\phi(\omega)$ is the phase change.

$$\implies lnr(\omega) = ln\rho(\omega) + i\phi(\omega)$$

where $ln\rho(\omega)$ is α_1 and $\phi(\omega)$ is α_2.

Applying the K-K relation, the phase change can be related to the reflectance by:

$$\phi(\omega) = \frac{-\omega.P}{\pi}\int_0^\infty \frac{lnR(s)}{s^2-\omega^2}ds \tag{16}$$

which can be written in a more useful form:

$$\phi(\omega) = \frac{-1}{2.\pi}\int_0^\infty ln \mid \frac{s+\omega}{s-\omega} \mid \frac{dlnR(s)}{ds}ds \tag{17}$$

Therefore, once we know the reflectance of a certain material, the phase change can be directly calculated using equation (17). In addition, the optical dielectric function $\varepsilon(\omega)$ with its real and imaginary parts $\varepsilon_1(\omega)$ and $\varepsilon_2(\omega)$ can also be obtained at every frequency ω using:

$$r(\omega) = \frac{\sqrt{\varepsilon(\omega)}-1}{\sqrt{\varepsilon(\omega)}+1} = \frac{n+ik-1}{n+ik+1}$$

$$\Longrightarrow \begin{cases} \varepsilon_1(\omega) &= n^2(\omega) - k^2(\omega) \\ \varepsilon_2(\omega) &= 2n(\omega)k(\omega) \end{cases} \tag{18}$$

Thus, the Kramers-Kronig technique permits the determination of these physical quantities from the measured reflectivity data only without the use of any fitting parameters. It is a direct, mathematical method with no physical modeling and assumptions.

As a summary of our work, the reflectivity coefficient can be separated into real and imaginary part r = A + iB where A and B are in terms of the index of refraction n and the extinction coefficient k. Once the measurements are done, they will be extrapolated to the low and high frequency end. We note here that the extrapolation of the reflectivity curve to 0 and infinity is done with the help of literature values [10, 13, 14]. The results are put in a Kramers-Kronig MATLAB code that gives the values of $\phi(\omega)$ from $R(\omega)$ (Eq. (17)). The values of $\rho(\omega)$ are just the square root of the reflectivity measurements that we have. So we obtain the equation:

$$r(\omega) = \rho(\omega)\exp(i\phi(\omega)) = \rho(\omega)cos(\phi) + i\rho(\omega)sin(\phi)$$

Finally, the two equations are equated as follows:

$$A + iB = \rho cos(\phi) + i\rho sin(\phi)$$

$$\Longrightarrow \begin{cases} A - \rho cos(\phi) &= 0 \\ B - \rho sin(\phi) &= 0 \end{cases} \tag{19}$$

The only unknowns in this system of two equations are the index of refraction and the extinction coefficient of the bulk material which will be obtained by equating these two equations using a MATLAB code that performs iterations on all the frequency range.

E. Numerical determination of *n* and *k*

After using Kramers-Kronig method to analyze the reflectivity spectra of 4H-SiC, 6H-SiC and to obtain the dielectric function $\varepsilon_{\parallel}$ and $\varepsilon_{\perp}$ for the different angles of incidence, we depict another technique that merges K-K results and Maxwell's equations to obtain the isotropic ordinary and extraordinary *n* near the bandgap edge. Theoretically speaking, $\varepsilon_{\perp}$ should be constant for all angles of incidence for the two polytypes of SiC [32]. Negligible discrepancy is noticed between the values of $\varepsilon_{\perp}$ for the different angles of incidence. As for $\varepsilon_{\parallel}$, it highly differs from one angle of incidence to the other. Therefore it is dependent on θ. The below method will permit the determination of isotropic $\varepsilon_{\parallel}$ as detailed later in this work. Subsequently, *n* and *k* will also be extracted independently of θ. The technique's detailed description is as follows:

First of all, the real and imaginary values of $\varepsilon_{\parallel}$ are given a minimum and a maximum value equal to -200 and 200 respectively. Next, a table is composed with all their possible values from -200 to 200 with a step of 0.8 (Table 2).

$\varepsilon_{\parallel}$	-200	-199.2	-198.4	...
$\varepsilon_{\perp}$				
-200	(-200,-200)	(-200,-199.2)	(-200,-198.4)	...
-199.2	(-199.2,-200)	(-199.2,-199.2)	(-199.2,-198.4)	...
-198.4	(-198.4,-200)	(-198.4,-199.2)	(-198.4,-198.4)	...
-197.6	(-197.6,-200)	(-197.6,-199.2)	(-197.6,-198.4)	...
-196.8	(-196.8,-200)	(-196.8,-199.2)	(-196.8,-198.4)	...
:	:	:	:	:

Table 2: Table containing all the possible combinations of real $\varepsilon_{\parallel}$ and imaginary $\varepsilon_{\parallel}$ from -200 to 200

The fixed given parameters are ω, R the set reflectivity values from the UV-VIS spectrophotometer, the real and imaginary parts of $\varepsilon_{\parallel}$ and of $\varepsilon_{\perp}$ from Kramers-Kronig,

and the incident angle θ. The formula relating $\varepsilon_{||}(\omega,\theta)$ to $\varepsilon_{||}(\omega)$ (independent of θ) is given by [32]:

$$\varepsilon_{||}(\omega,\theta) = \frac{\varepsilon_{\perp}(\omega)\varepsilon_{||}(\omega)}{\varepsilon_{\perp}(\omega)\sin^2\theta + \varepsilon_{||}(\omega)\cos^2\theta} \tag{20}$$

The real and imaginary part of both sides of the equation are equated to zero. The unknown is $\varepsilon_{||}(\omega)$. Then, for each ω, all the pairs of numbers in the above table are tested to see which ones (we could have more than one solution) are the roots to the two equations. After filtering out all the possible solutions for each frequency, we insert them, one by one, in the expression of the reflectivity R in terms of the incident angle θ and the dielectric function ε:

$$R_{||} = r_{||}r_{||}^{*}$$

where $r_{||}$ is given by [30]:

$$r_{||} = \frac{\cos(\theta) - \sqrt{\varepsilon_{||} - \sin^2\theta}}{\cos(\theta) + \sqrt{\varepsilon_{||} - \sin^2\theta}} \tag{21}$$

We then calculate the difference between R calculated and R measured. The pair of real and imaginary values that gives closest result to zero will be considered as the only best solution for this frequency. After checking for the range of frequency around the bandgap, we will acquire the set of solutions that represent $\varepsilon_{||}(\omega)$. Finally, we make use of the relation between $\varepsilon_{||}(\omega)$, $n_{||}$ and $k_{||}$ to extract the isotropic extraordinary n and extinction coefficient k around the bandgap:

$$\begin{cases} n_e &= \frac{1}{\sqrt{2}}\sqrt{\varepsilon_1(\omega) + \mid \varepsilon(\omega) \mid} \\ k_e &= \frac{1}{\sqrt{2}}\sqrt{-\varepsilon_1(\omega) + \mid \varepsilon(\omega) \mid} \end{cases} \tag{22}$$

(keeping in mind that ε_1 is the real part of ε. See Eq. 18.) The same relation is used to extract the ordinary index of refraction $n_{\perp}$ and $k_{\perp}$ from $\varepsilon_{\perp}$.

CHAPTER IV

RESULTS AND DISCUSSION

In this chapter, we describe the results obtained on the optical characterization of the samples. In the first section, we show the graphs of the reflectivity measurements vs energy for each angle, each polarization, of each polytype. In the second section, we present the results of n and k deduced from Kramers-Kronig method for each angle, for the two polarizations, for each polytype. In the third section, we show how we deduce the behavior of the isotropic ordinary and extraordinary n and k as a function of energy of SiC near the bandgap edge of its two polytypes. In the last section, we compare our results to those published in the literature and assess the validity of our technique.

A. Reflectivity Measurement

1. p-polarized light

The reflectivity spectra of 4H-SiC and 6H-SiC, for each angle of incidence from 10 to 60 ° for p-polarized light, is plotted in Figures 9 and 10, respectively:

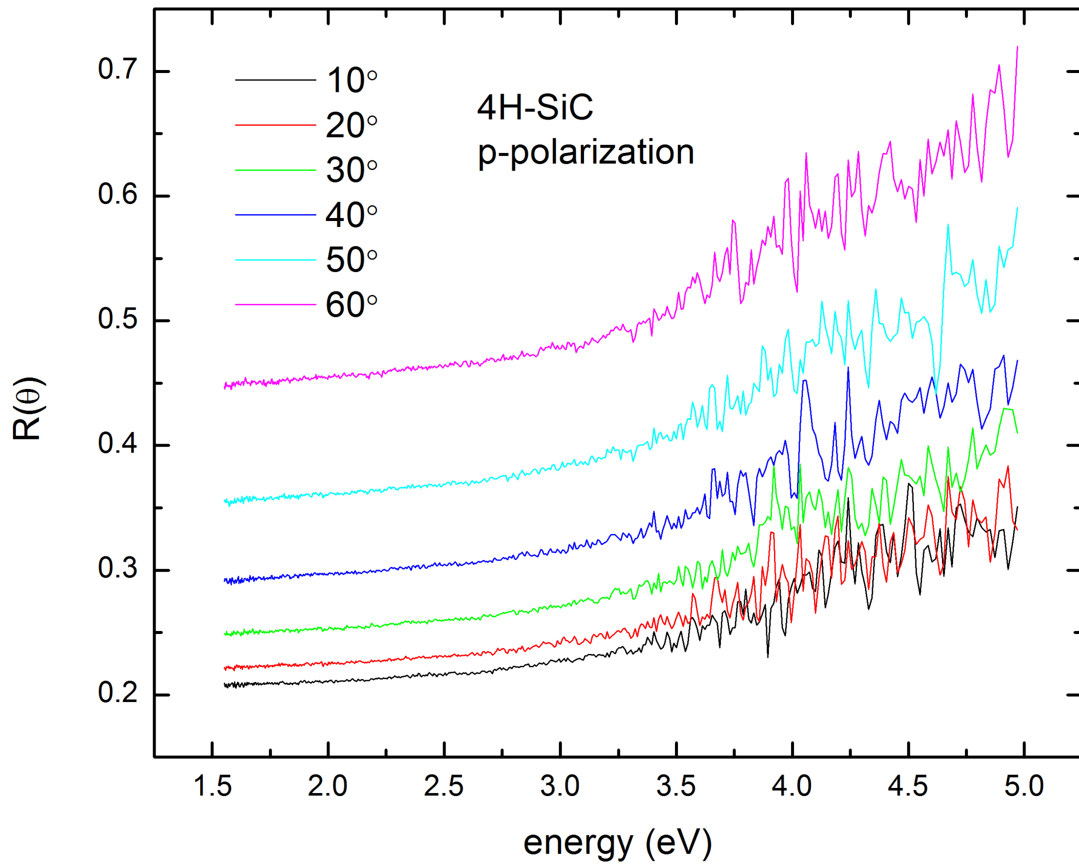

Figure 9: Reflectivity of p-polarized light for 4H-SiC at the different angles of incidence

The reflectivity spectra shows an increasing function for all the angles. The reflectivity R starts at 0.2 for 10°. This value increases to 0.22, 0.25, 0.29, 0.35, 0.44 as we increase the angle of incidence to 20, 30, 40, 50 and 60 ° respectively.

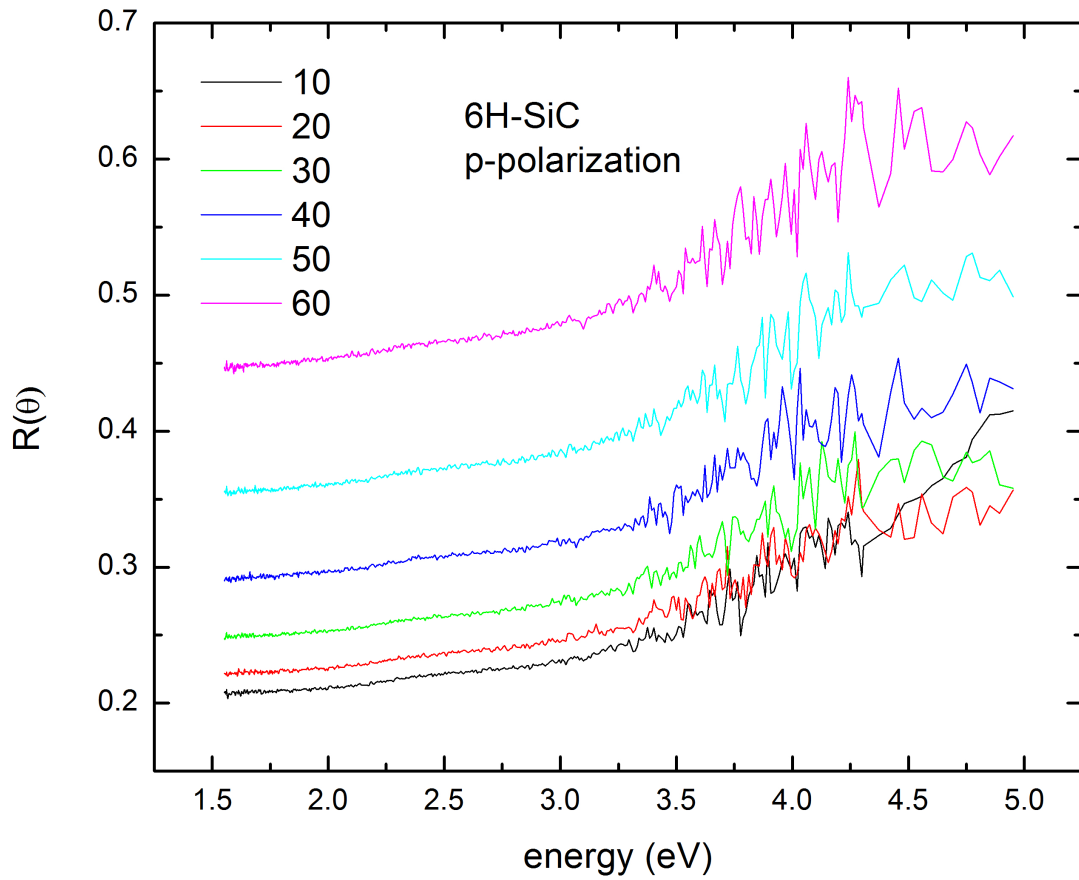

Figure 10: Reflectivity of p-polarized light for 6H-SiC at the different angles of incidence

Similar to 4H-SiC, the reflectivity spectra of 6H-SiC increases as energy increases. Also, the initial point of the spectra is 0.2 for 10° and increases to 0.22, 0.25, 0.29, 0.35, 0.45 for 20, 30, 40, 50 and 60 ° respectively. We can notice the similar beginning values of R for the two polytypes of SiC for the p-polarized light when **E** is parallel to the c-axis.

2. s-polarized light

The reflectivity spectra of 4H-SiC and 6H-SiC for each angle of incidence is plotted in Figures 11 and 12 respectively:

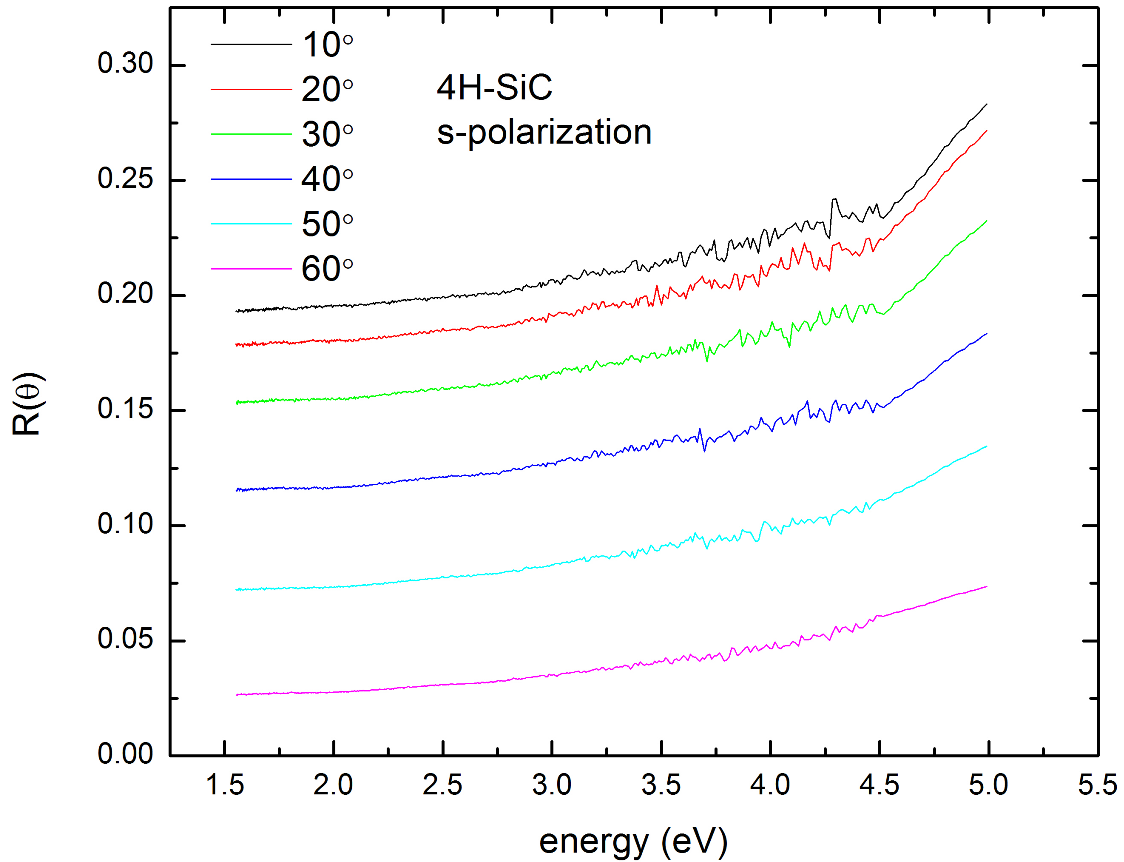

Figure 11: Reflectivity of s-polarized light for 4H-SiC at the different angles of incidence

The reflectivity spectra displays an increasing function of energy identical to the case of p-polarized light. The initial point of the spectra is at 0.19 for 10 °, and contrary to the p-polarized light behavior, decreases to 0.18, 0.15, 0.87, 0.072, 0.026 for 20, 30, 40, 50 and 60 ° respectively.

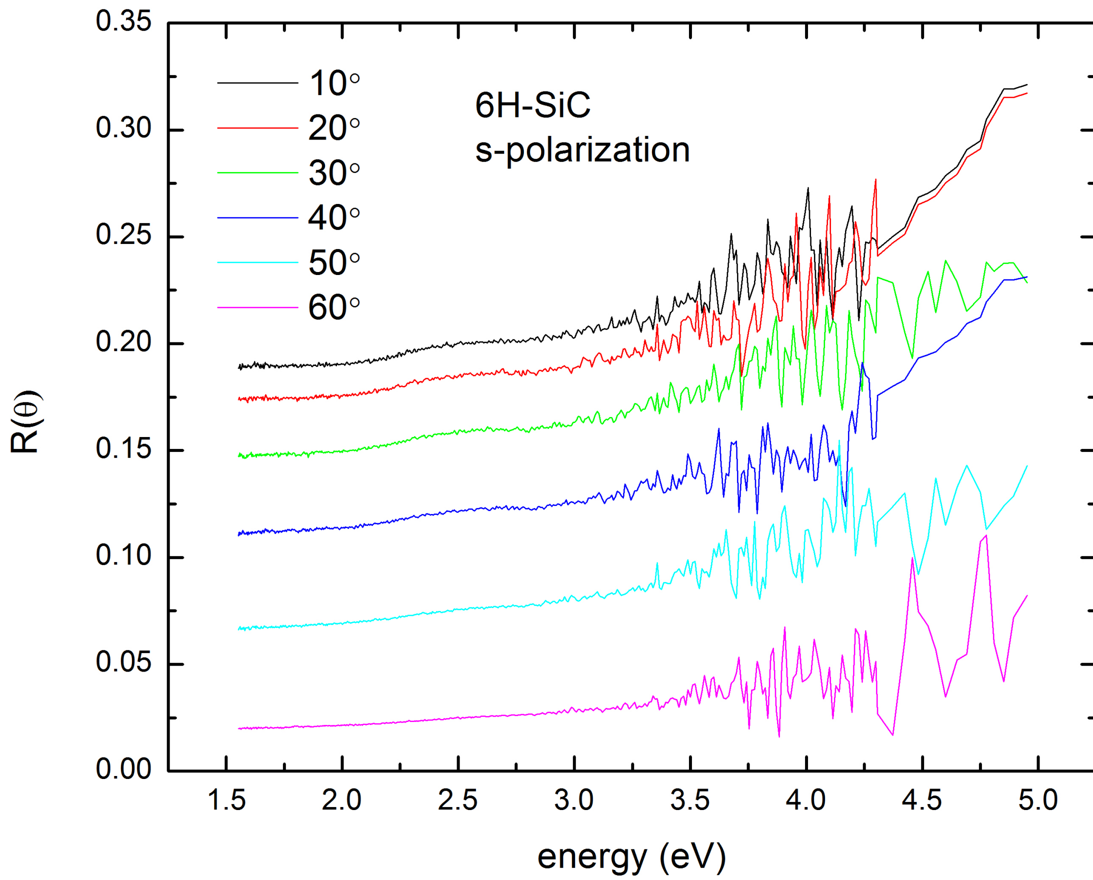

Figure 12: Reflectivity of s-polarized light for 6H-SiC at the different angles of incidence

Analogous to the case of 4H-SiC, the reflectivity curve increases with energy. Also the starting point decreases from 0.19 at 10° to 0.17, 0.15, 0.11, 0.066, 0.02 for 20, 30, 40, 50 and 60 ° respectively. We did not observe any feature around the bandgap (3.0 for 6H-SiC and 3.2 for 4H-SiC) since these two polytypes are indirect bandgap semiconductors. The transition of the electron from the valence band to the conduction band is highly improbable. Therefore we can only see the reflectivity increasing steadily as energy increases from 1.5 to 5 eV.

B. Determination of *n* as a function of energy

We now present the results of the index of refraction *n* extracted from Kramers-Kronig method for the two polytypes, at the various angles of incidence, for the p and s polarization.

1. p-polarized light

As mentioned in chapter 3, the Kramers-Kronig method will help to extract the index of refraction dependent on the angle of incidence for all the frequency range. Figures 13 and 14 display *n* vs energy graph of 4H-SiC and 6H-SiC respectively.

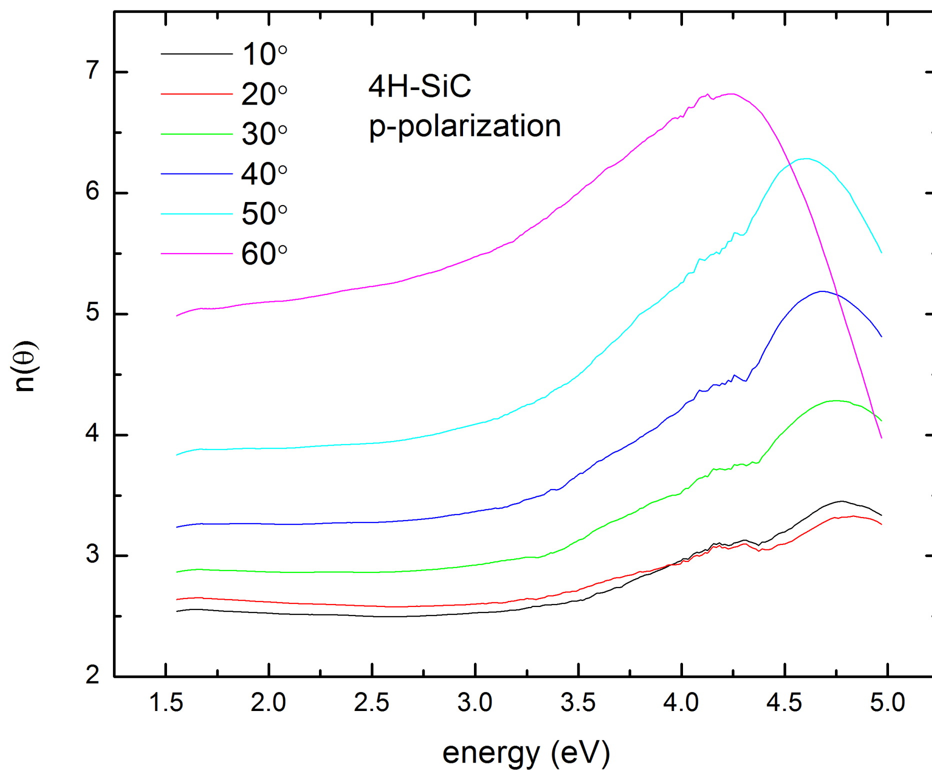

Figure 13: *n* vs energy of p-polarized light for 4H-SiC at the different angles of incidence (after 120 points smoothing)

The graph increases, for all angles, for the energy between 1.5 and 4.5 eV then decreases slightly when the energy reaches 5 eV. *n* starts at 2.54 for 10 ° and increases to reach 2.64, 2.87, 3.24, 3.83, 4.98 for 20, 30, 40, 50 and 60 °. The peak at 4.5 eV could be due to the resonance between the incident light and excitons in the material.

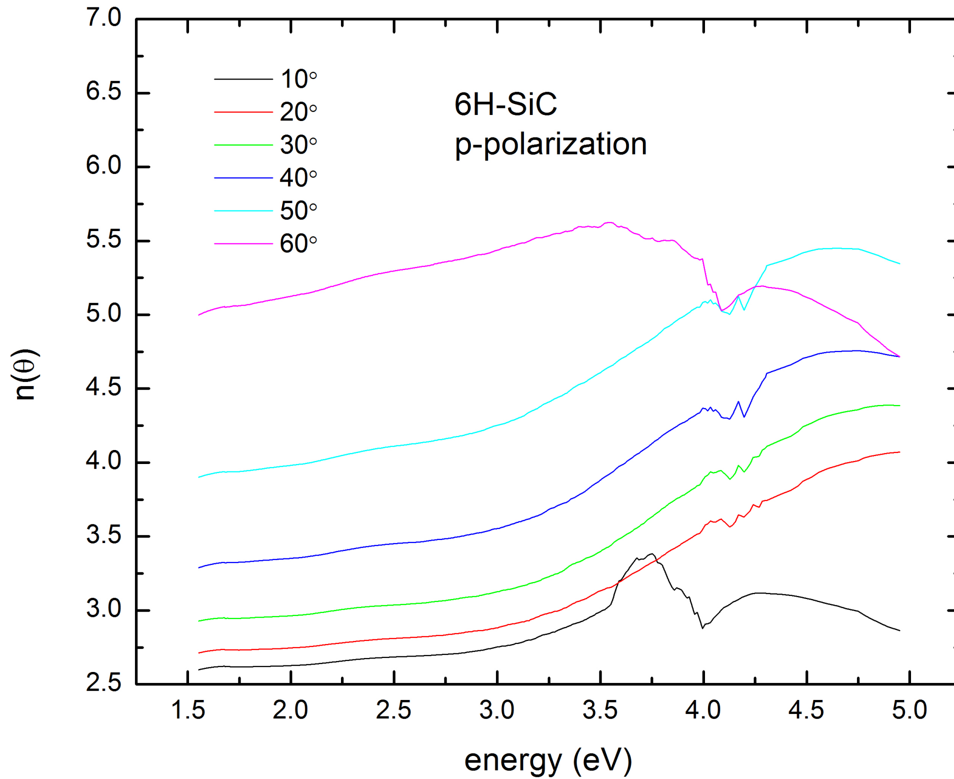

Figure 14: *n* vs energy of p-polarized light for 6H-SiC at the different angles of incidence (after 120 points smoothing)

The graph increases for all angles when the energy goes from 1.5 to 5 eV. Similar to 4H-SiC, the initial point of n is 2.6, 2.71, 2.93, 3.29, 3.9, 5 for 10, 20, 30, 40, 50 and 60°.

2. s-polarized light

Figures 15 and 16 show *n* versus energy of 4H-SiC and 6H-SiC:

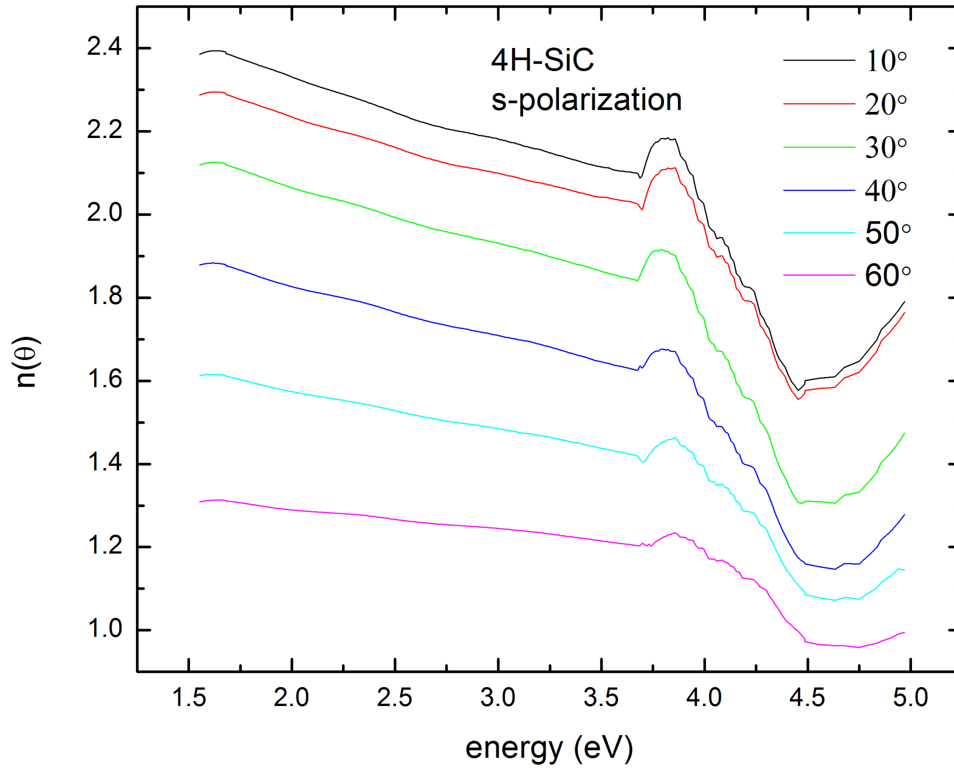

Figure 15: *n* vs energy of s-polarized light for 4H-SiC at the different angles of incidence (after 120 points smoothing)

Contrary to the case of p-polarized light, *n* decreases for all angles when energy ranges from 1.5 to 5 eV. The initial points of *n* decrease from 2.38 to 2.29, 2.12, 1.88, 1.61, 1.31 as the angle of incidence is increased from 10 to 20, 30, 40, 50 and 60° respectively.

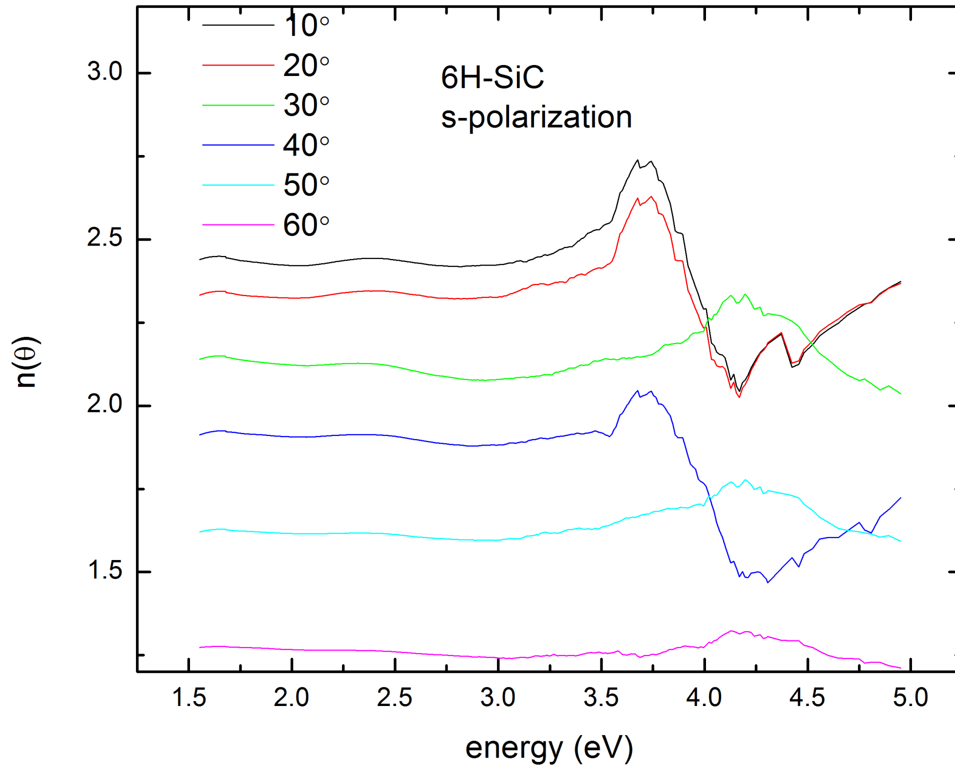

Figure 16: *n* vs energy of s-polarized light for 6H-SiC at the different angles of incidence (after 120 points smoothing)

The graphs increase till they reach a peak at 3.75 eV for the angle of 10, 20 and 40°. At 30, 50 and 60 ° the curve sightly increases to a peak at 4.25 eV. Similar to 4H-SiC, n starting values decrease from 2.44 to 2.33, 2.14, 1.91, 1.62, 1.27 as the angles of incidence increase from 10 to 20, 30, 40, 50 and 60° respectively. The peaks at 3.75 eV result from resonance due to excitons or defects in the sample.

C. Determination of *k* as a function of energy

We now present the results of the determination of the extinction coefficient *k* extracted from Kramers-Kronig method for the two polytypes, at the various angles of

incidence, for the p and s polarization.

1. p-polarized light

Figures 17 and 18 exhibit k vs energy curve for 4H-SiC and 6H-SiC respectively:

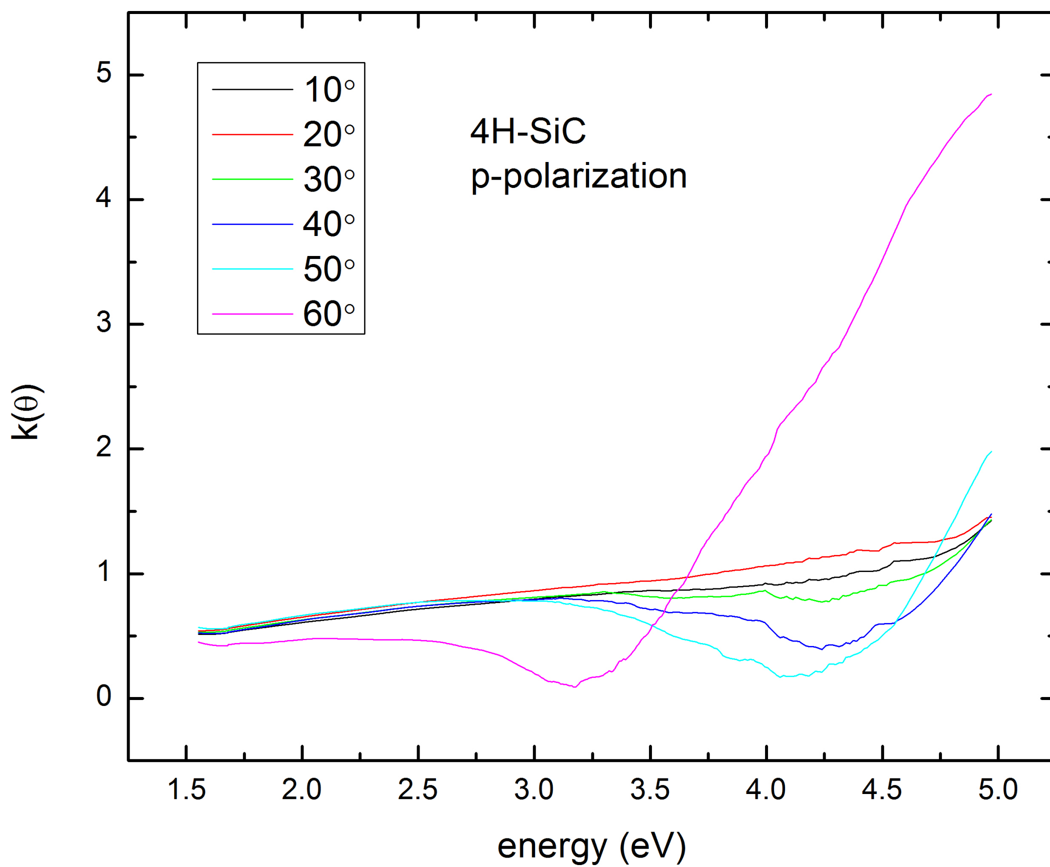

Figure 17: k vs energy of p-polarized light for 4H-SiC at the different angles of incidence (after 120 points smoothing)

It is noticed that the k values are identical (equal to 0.5) for all angles (except 60°) in the energy range 1.5-3.25 eV.

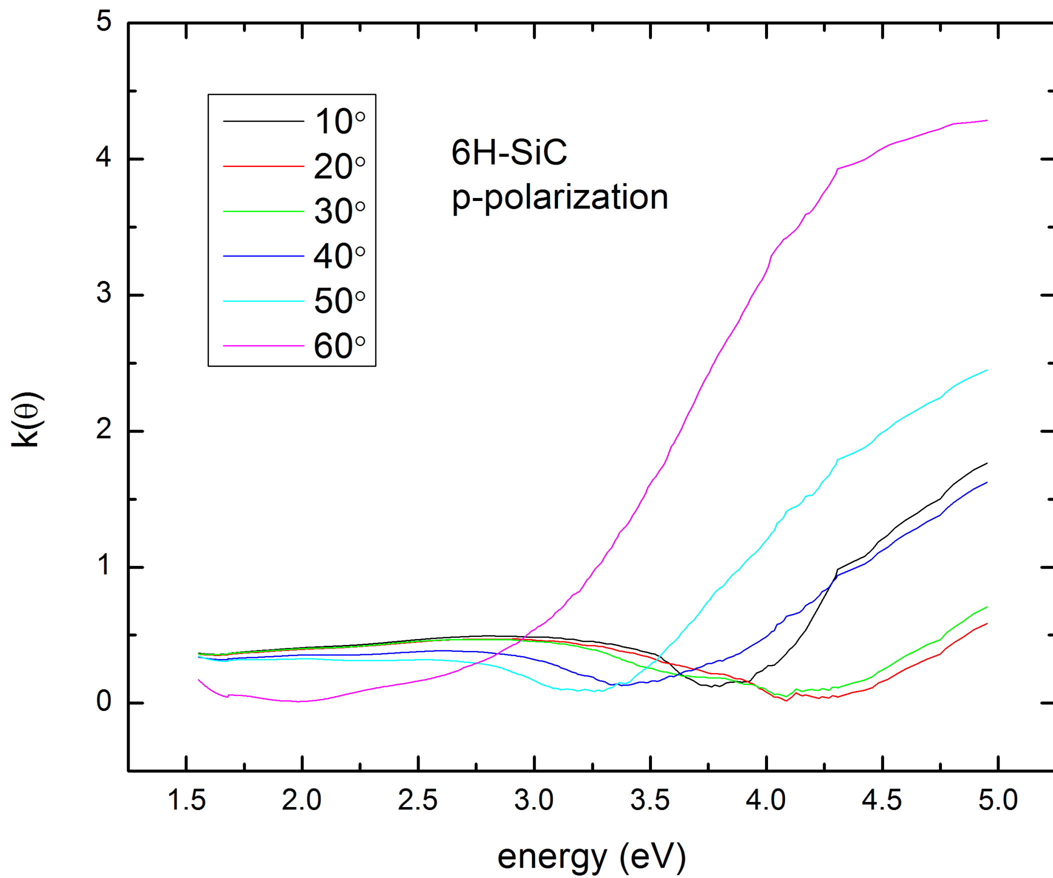

Figure 18: *k* vs energy of p-polarized light for 6H-SiC at the different angles of incidence (after 120 points smoothing)

Analogous to the case of 4H-SiC, the *k* values start at the same point (around 0.36) for all angles except 60° (0.17).

2. s-polarized light

Figures 19 and 20 depict the curve of *k* vs energy for 4H-SiC and 6H-SiC respectively.

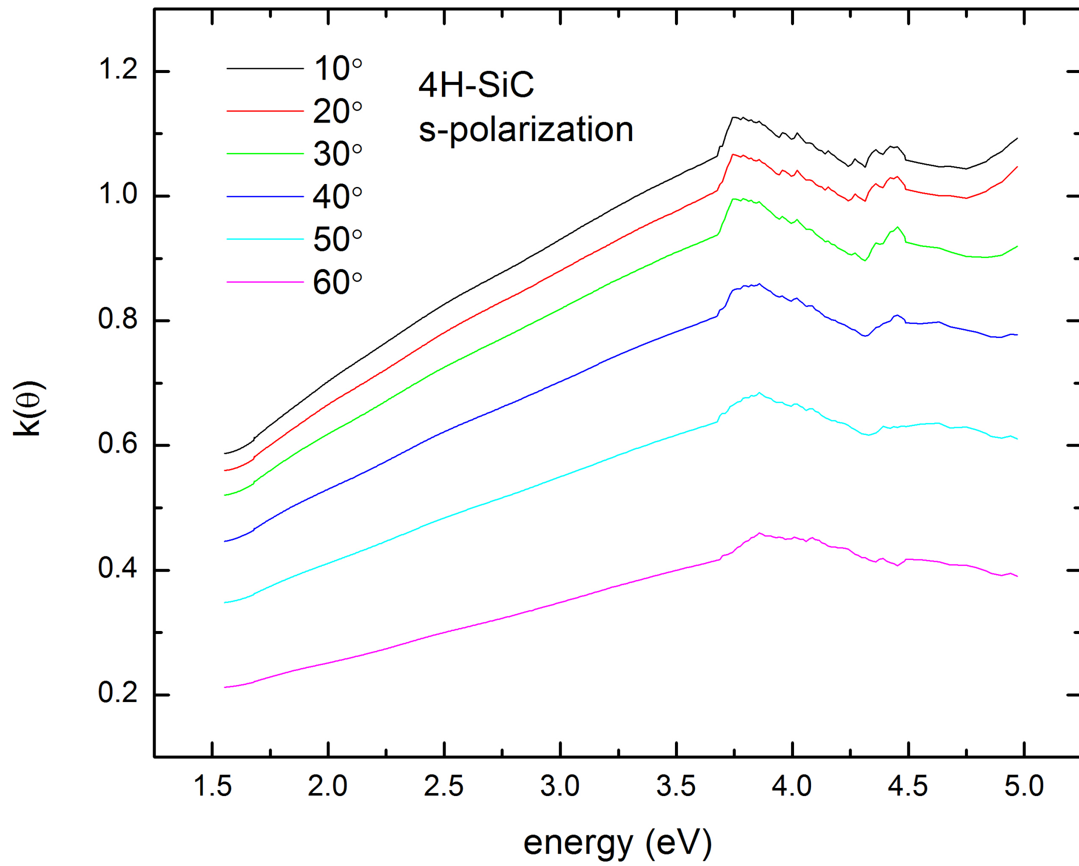

Figure 19: k vs energy of s-polarized light for 4H-SiC at the different angles of incidence (after 120 points smoothing)

For s-polarized light and at all angles, k increases with energy but the initial values of k change from 0.59 to 0.21 as the angle is varied from 10 to 60°.

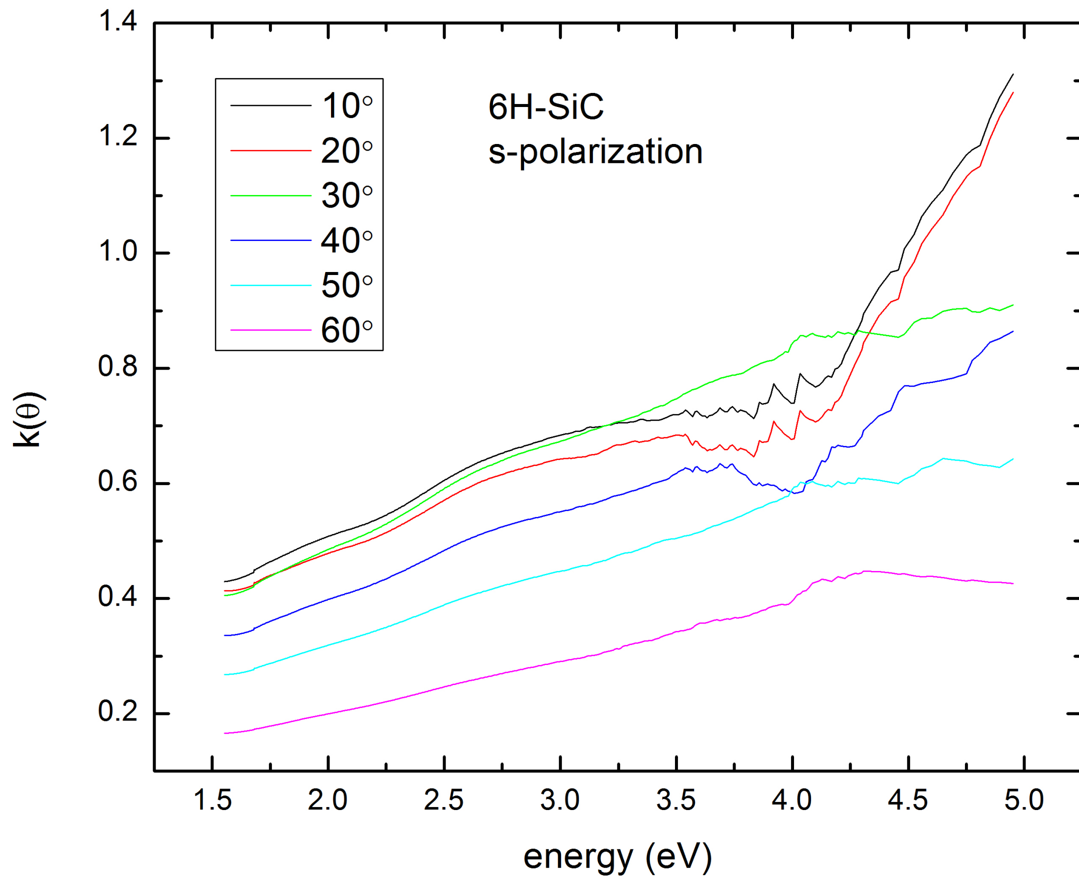

Figure 20: *k* vs energy of s-polarized light for 6H-SiC at the different angles of incidence (after 120 points smoothing)

Identical to 4H-SiC, *k* increases as energy increases. *k* initial point is at 0.43 and at 0.16 as the angle is changed from 10 to 60°.

D. Determination of the isotropic *n* and *k*

As explained in the previous chapter, isotropic ordinary and extraordinary *n* and *k* are extracted, with the help of the new experimental technique, around the bandgap energy of the two polytypes.

1. 4H-SiC

We now show in Figure 21 the results of ordinary and extraordinary *n* of 4H-SiC around the bandgap edge:

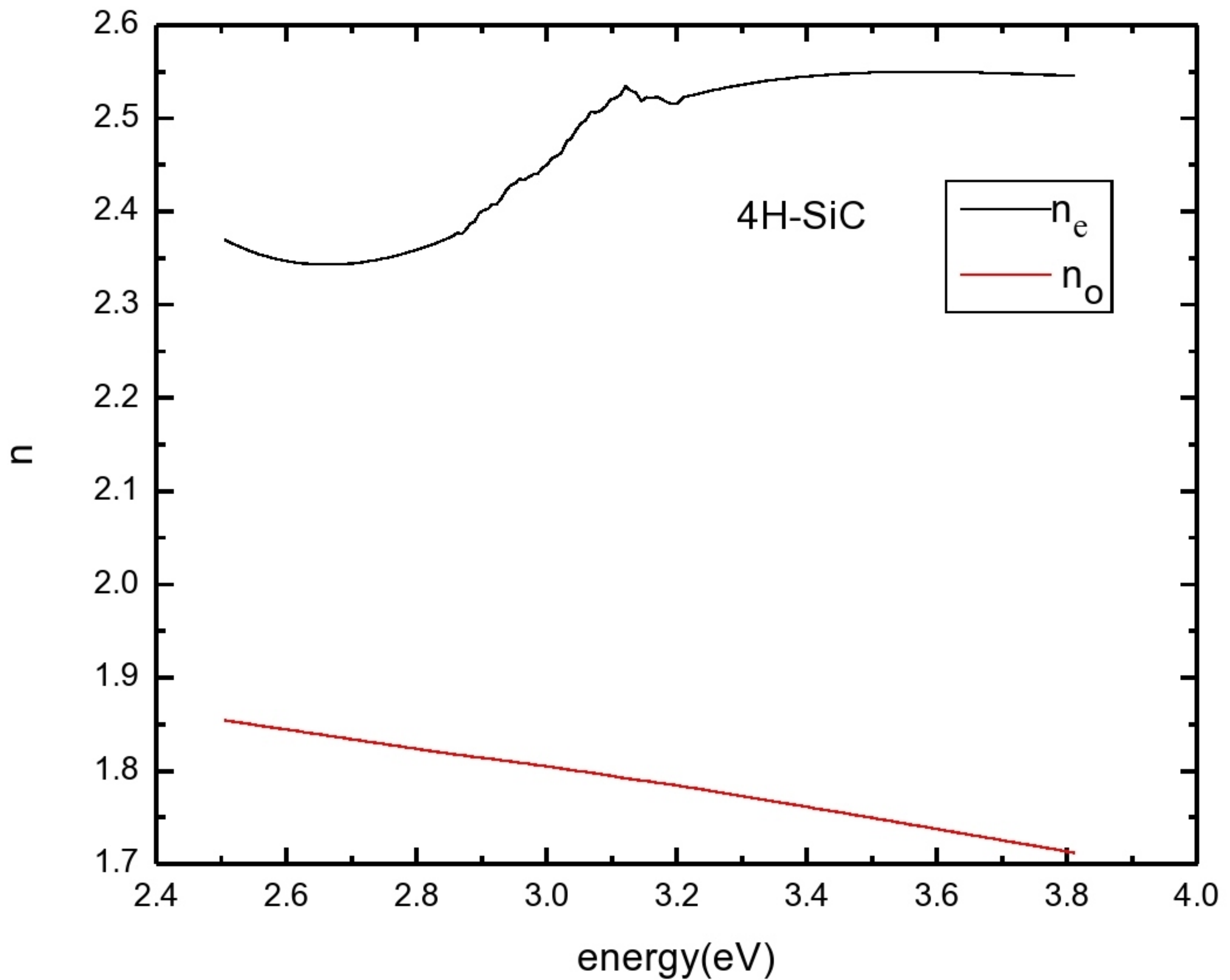

Figure 21: ordinary and extraordinary *n* vs energy of 4H-SiC around the bandgap = 3.2 eV

The value of the extraordinary n_e makes a response around the indirect bandgap (=3.2eV) while the ordinary n_o decreases steadily as energy increases from 2.5 to 3.8 eV.

The results for ordinary and extraordinary *k* are considered in Figure 22:

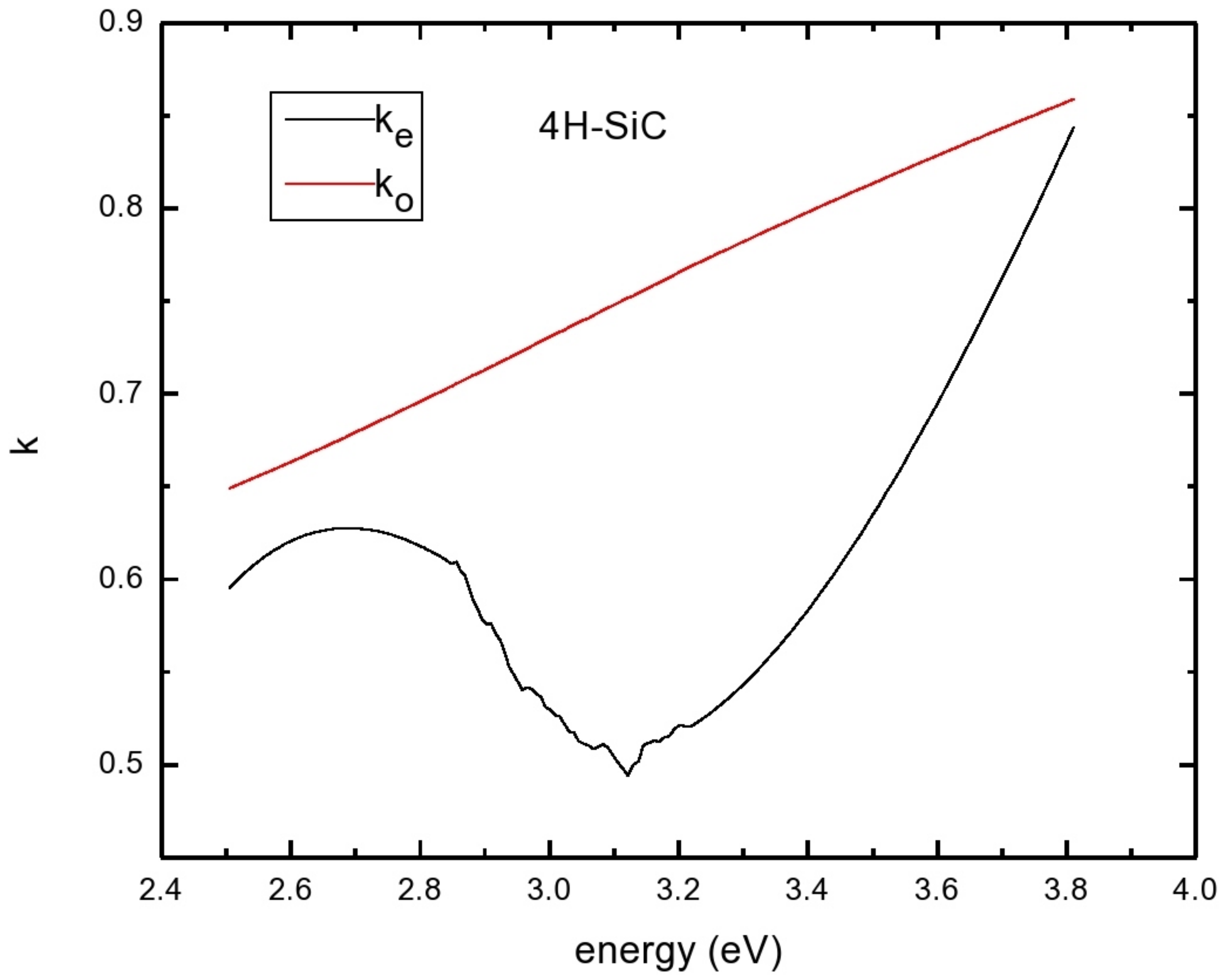

Figure 22: ordinary and extraordinary *k* vs energy of 4H-SiC around the bandgap = 3.2 eV

The value of the extraordinary k_e has a minimum at E=3.2eV while the ordinary k_o maintains a steady increase for E between 2.5 and 3.8 eV.

2. 6H-SiC

Figure 23 is the curve of the ordinary and extraordinary *n* vs energy for 6H-SiC:

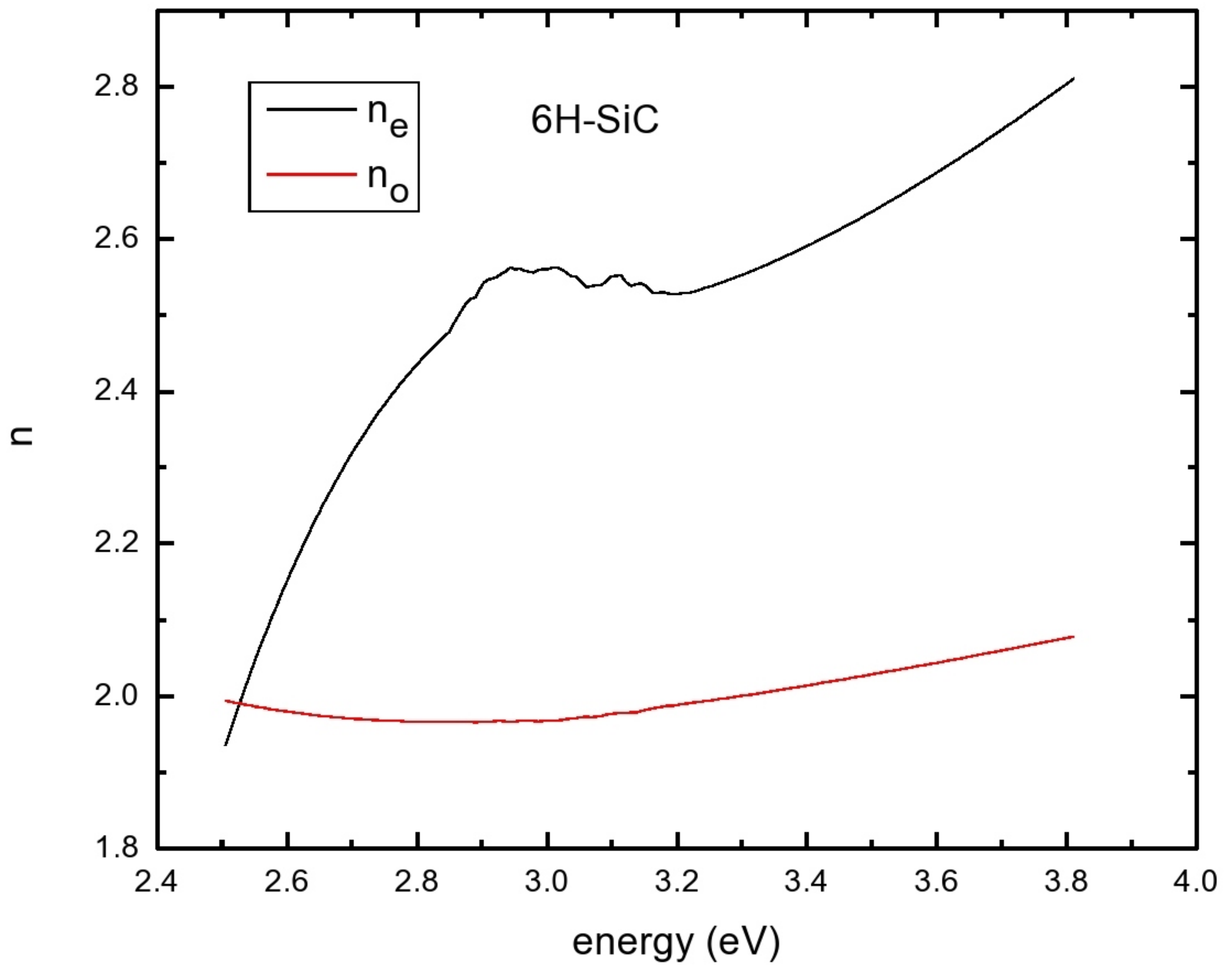

Figure 23: ordinary and extraordinary *n* vs energy of 6H-SiC around the bandgap = 3.0 eV

The increasing function of extraordinary n_e shows a horizontal behavior around the indirect bandgap (=3.0 eV). Ordinary n_o slightly decreases at the bandgap then increases as energy increases.

Figure 24 is the curve of ordinary and extraordinary *k* for 6H-SiC:

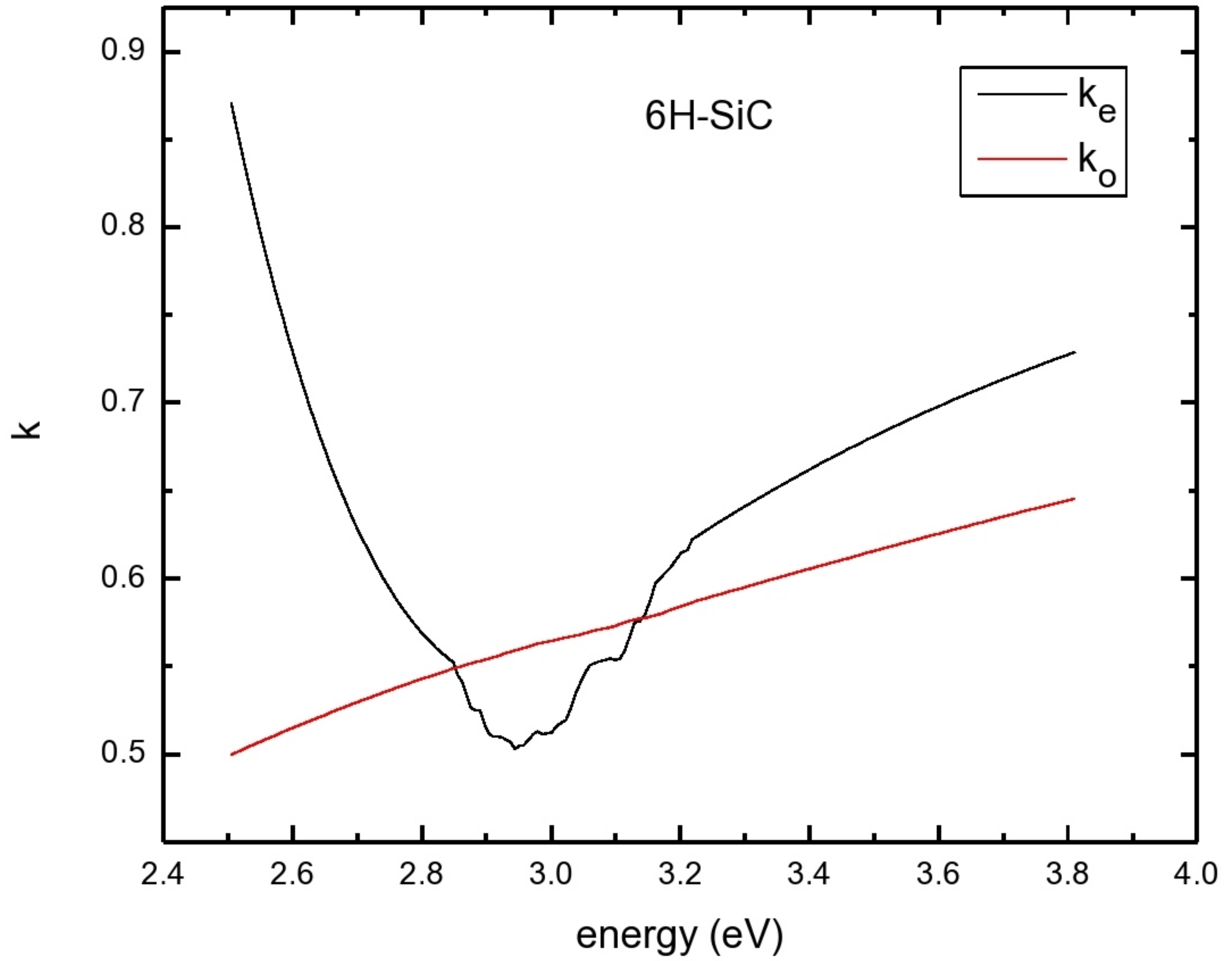

Figure 24: ordinary and extraordinary k vs energy of 6H-SiC around the bandgap = 3.0 eV

Also, the extraordinary k_e displays a minimum at the bandgap (=3.0eV) while the ordinary k_o increases steadily with energy.

In summary, the extraordinary components of n and k (where **E** is $\|$ to the c axis) exhibit an obvious response around the indirect bandgap of 4H- and 6H-SiC. However, the ordinary components (where **E** is $\perp$ to the c axis) show a change as they pass the indirect bandgap energy. This result is in confirmation with what Lindquist and co-workers [19] reported in their paper that effects of polytypism are more highlighted when **E** is parallel to the c axis because the stacking layers of Si and C atoms are different in the direction

parallel to the c axis.

E. Comparison with literature

In order to overcome the analysis issues encountered in the commonly used approaches of previous papers (See chapter 2), we analyze the reflectivity spectra by using our approach, which is outlined in chapter 3. This approach consists on a direct conversion of the reflectivity spectrum to frequency-dependent dielectric properties without any physical modeling. It provides the exact dielectric properties of the measured sample in the measured frequency range, and takes into account the contribution of defects related excitations in the measured sample without the need of any theoretical convolution tools.

1. Dielectric function

The ordinary and extraordinary dielectric properties of 4H-SiC and 6H-SiC as derived from our approach are shown in Figures 25 and 26 together with previously reported data.

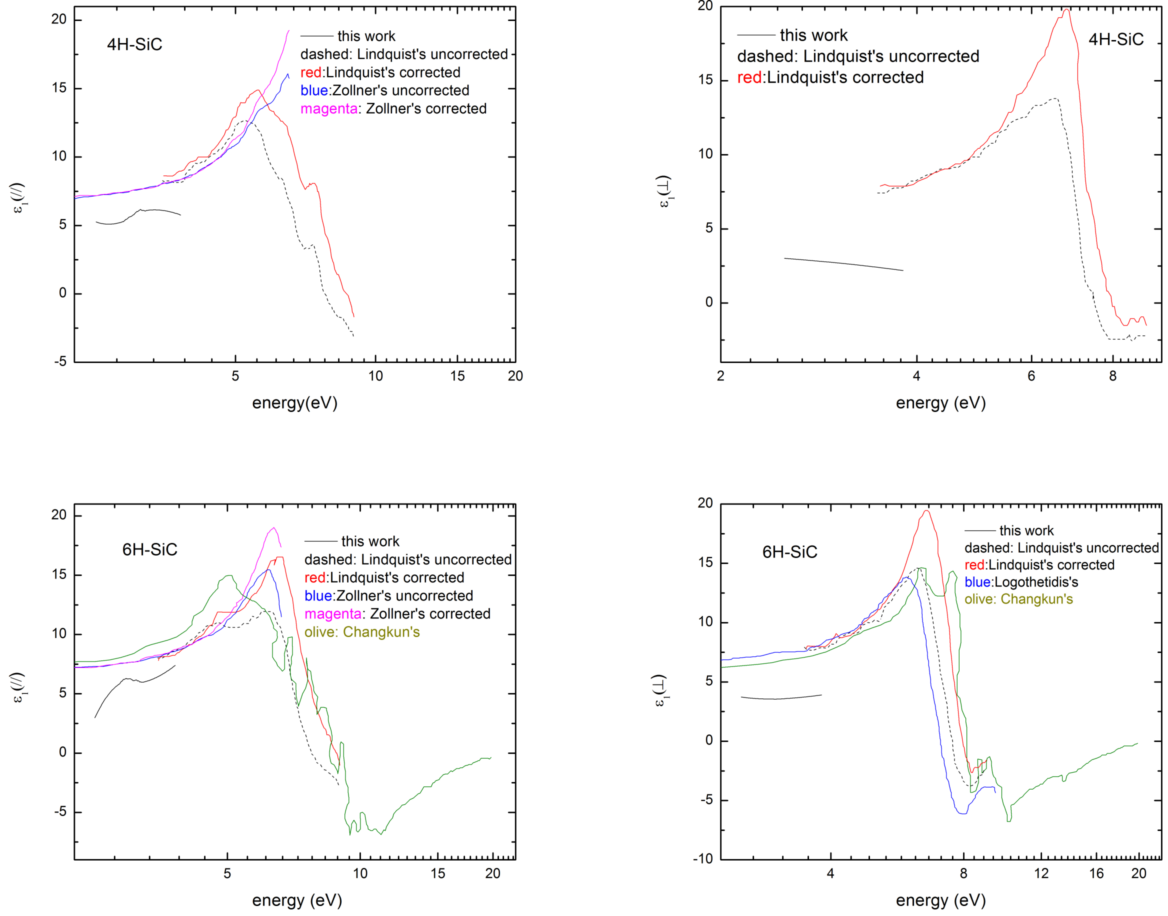

Figure 25: The real parts of ordinary and extraordinary dielectric function as compared to previously reported values

The real parts of the ordinary and extraordinary dielectric functions of both 4H-SiC and 6H-SiC obtained from our approach are compared to the results of Lindquist et al. [19] that are obtained from ellipsometry spectroscopy and corrected by removing the contribution of the dioxide silicon layer from the sample surface, and those of Zollner et al. [17] that are obtained from first principles calculations. Our results show lower values in all cases. This may be due to the fact that first principles calculations assume defect-free lattice, and consequently ignore possible contributions of defects response that may interfere with the host lattice response and lower the real part of the dielectric function. Similarly, ellipsometry analysis often results in an overestimation of the real part of the dielectric function because ellipsometry spectra are usually described by models

that do not properly describe the oscillators damping, which may lower the real part of the dielectric function.

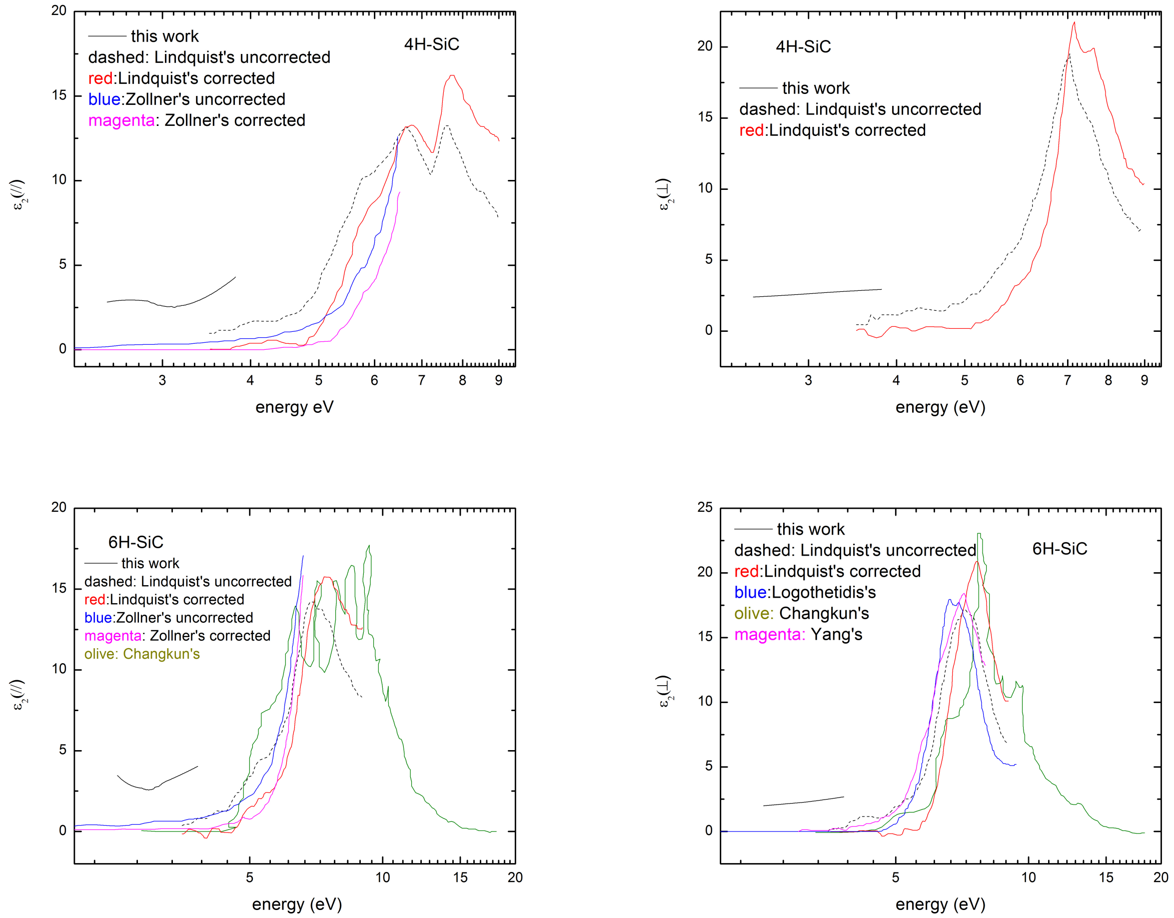

Figure 26: The imaginary parts of ordinary and extraordinary dielectric function as compared to previously reported values

The ordinary and extraordinary imaginary parts of the dielectric functions of both 4H-SiC and 6H-SiC obtained from our approach are also compared to the results of Lindquist et al.[19] and Zollner et al. [17]. As can be noticed, our results show higher values in all cases. This can be understood if we keep in mind that the existence of defects in a host crystal enhances the material's absorption of light in a wide spectral range, and thus enhances the imaginary part of the dielectric function in a wide spectral range. As our approach directly converts the reflectivity data to the dielectric properties of the measured sample without any physical modeling, it accounts for the enhanced absorption

due to defects. However, the ellipsometry analysis and first principle calculations do not account for any defects contributions, and therefore underestimate the imaginary part of the dielectric function of a sample containing defects.

2. *Index of refraction*

The refraction index obtained from our approach is compared to the results of Adolph et al. [22] that are obtained from first principles calculations and the results of Susumu et al. [23] that are obtained from ellipsometry spectroscopy (Figure 27):

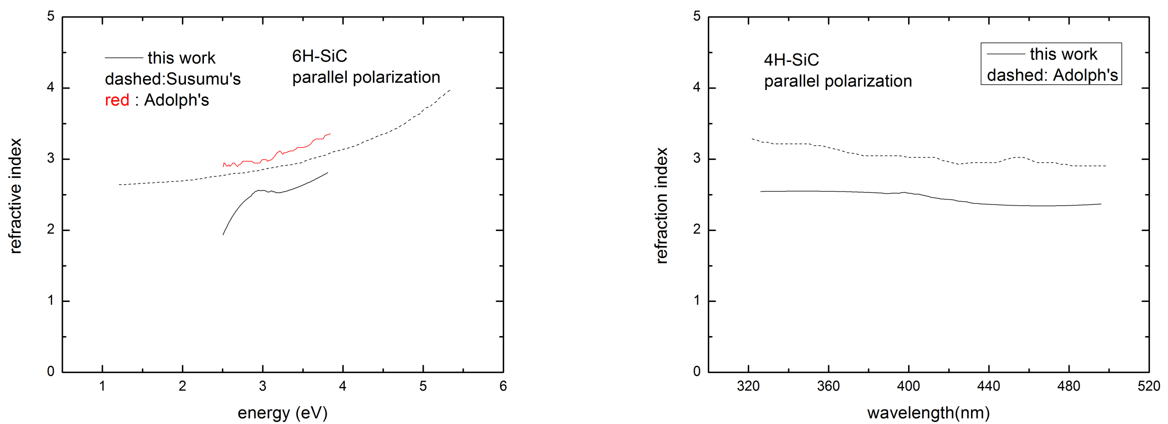

Figure 27: The extraordinary refractive index compared to previously reported values

Again, our approach provides lower values for the refraction index than first principles calculation and ellipsometry spectroscopy. As highlighted previously, this disagreement between our results and previously reported results is due to the fact that our approach account for the contribution of defects to the overall material optical properties, while ellipsometry spectroscopy and first principle calculations ignore such an effect.
For the sake of verification of the reliability of the used reflectivity-based technique for the determination of the dielectric properties and the convergence of the associated numerical code, we back calculated the reflectivity spectra at normal incidence by using the

deduced dielectric properties of the measured samples, and compared the results to the measured reflectivity spectra. The results for 4H-SiC and 6H-SiC are shown in Figure 28:

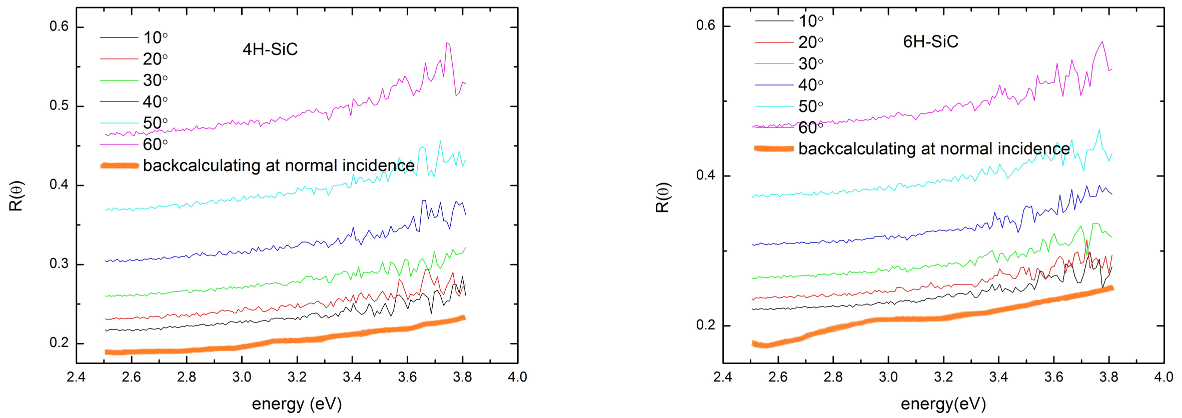

Figure 28: The reflectivity spectra at normal incidence by using the deduced dielectric function

For both 4H-SiC and 6H-SiC, the calculated normal incidence reflectivity spectrum matches with the trend of the dependence of the light angle of incidence on the reflectivity spectra. This clearly demonstrates the accuracy of the developed technique in describing the exact ordinary and extraordinary dielectric properties of the measured sample. We have thus deduced the dielectric properties and optical parameters of 4H-SiC and 6H-SiC by using a reflectivity-based technique that involves no physical modeling and free of adjustable parameters. Since crystal impurities, disorder, strain, and different free carrier density can affect significantly the dielectric parameters, the disagreement between our results and the previously reported data that were obtained by using either ellipsometry spectroscopy or first principles calculations can be explained by the contribution of defects to the dielectric properties that is accounted for in our approach and ignored when ellipsometry and first principle calculations are used.

CHAPTER V

CONCLUSION AND FUTURE WORK

In this thesis, we undertook the task of determining experimentally the optical properties, n and k, of the most common encountered bulk silicon carbide polytypes 4H- and 6H-SiC, around the bandgap edge.

We used the UV-VIS spectrophotometer to get sets of reflectivity data as a function of energy, one for p-polarized light and one for s-polarized light, for each SiC polytype at various incident angles, 10 to 60°. In both cases, no feature was detected around the indirect bandgap so the reflectivity spectrum, as expected, increases steadily as the energy increases.

From these measurements, and by using a Kramers-Kronig approach, we then determined n and k as a function of θ along with the real and imaginary parts of ε. It was found that, for p-polarized light, n increases as θ increases for the two polytypes. Moreover, n smoothly increases as a function of energy for all angles of incidence. For s-polarized light, the initial values of n increase as θ increases for the two polytypes, but n smoothly decreases in function of energy for a fixed value of θ.

The isotropic n and k were then computed around the bandgap energy of both polytypes. For 4H-SiC, the extraordinary n_e vs energy increases with energy and shows a response at 3.2 eV (bandgap value) while the ordinary n_o decreases steadily as a function of energy. The extraordinary k_e exhibits a minimum at 3.2 eV whereas ordinary k_o maintains an increasing function of energy.

For 6H-SiC, the extraordinary n_e increases with energy but shows an inflexion point at 3.0 eV (bandgap value) while the ordinary n_o shows a broad minimum. The extraordinary k_e has a minimum at 3.0 eV while the ordinary k_o increases for all energy values.

These conclusions, are in agreement with what is known of the SiC structural stacking sequence. Si-C stacking layers mostly differ in the direction parallel to the c-axis. This is proven from the extraordinary components of n and k that respond to the indirect bandgap more than ordinary components do, thus accounting for the greater anisotropy of 4H- and 6H-SiC in the direction parallel to the c axis.

After a comparison is established between the ε values drawn from our method and the experimentally and theoretically fitted ε values of previous works, it can be shown that ellipsometry methods and first-principle calculations overestimate the real part of ε and underestimate its imaginary part. This can be explained by the fact that these techniques do not account for defects, disorder, strain, and different free carrier density in the sample under study. Similar arguments are given to explain the discrepancy observed between our index of refraction data and previous reports. Finally, to validate the reliability of the method used in this work, we back calculated the reflectivity spectra at normal incidence from the calculated ε. It shows an analogous trend to the reflectivity spectra obtained from non-zero angles, thus confirming the validity of our developed technique.

Future work could deal with the application of our new technique to other polytypes of SiC such as 3C- and 15R-, and to more purified samples of 4H- and 6H-SiC, on a wider wavelength range, so that better comparisons can be formed with other methods such as spectroscopic ellipsometry and first-principle calculations.

BIBLIOGRAPHY

[1] AH. Rashed. Properties and characteristics of silicon carbide. *POCO Graphite Inc., Decatur*, 2002.

[2] T. Ayalew. *SiC semiconductor devices technology, modeling and simulation.* 2004.

[3] A. Taylor and RM. Jones. Silicon carbide - a high temperature semiconductor. In *Proc. Conf. on Silicon Carbide (Boston, MA 1959)*, pages 147–54, 1960.

[4] GL. Harris. *Properties of Silicon Carbide*. 1995.

[5] M E. Levinshtein, S L. Rumyantsev, and M S. Shur. *Properties of Advanced Semiconductor Materials: GaN, AIN, InN, BN, SiC, SiGe*. 2001.

[6] H. Abderrazak and E. Hmida. Silicon carbide: Synthesis and properties. *Properties and applications of silicon carbide, InTech, Rijeka (Croatia)*, pages 351–388, 2011.

[7] P. Masri. Silicon carbide and silicon carbide-based structures: the physics of epitaxy. *Surface Science Reports*, 48:1–51, 2002.

[8] G. Wellenhofer and U. Rössler. Global band structure and near-band-edge states. *Physica Status Solidi (b)*, 202:107–123, 1997.

[9] Philip G Neudeck. Silicon carbide technology. *The VLSI Handbook*, pages 1–5, 2006.

[10] S. Logothetidis and J. Petalas. Dielectric function and reflectivity of 3c-sic and the component perpendicular to the c axis of 6h-sic in the energy region 1.5-9.5 ev. *Journal of Applied Physics*, 80:1768–1772, 1996.

[11] BE. Wheeler. The ultra-violet reflectivity of α and β sic. *Solid State Communications*, 4:173–175, 1966.

[12] VI. Gavrilenko, SI. Frolov, and NI. Klyui. Electronic band structure and optical properties of cubic silicon carbide crystals. *Physica B: Condensed Matter*, 185:394–399, 1993.

[13] WRL. Lambrecht, B. Segall, W. Suttrop, M. Yoganathan, RP. Devaty, WJ. Choyke, JA. Edmond, JA. Powell, and M. Alouani. Optical reflectivity of 3c and 4h-sic polytypes: Theory and experiment. *Applied physics letters*, 63:2747–2749, 1993.

[14] WRL. Lambrecht, B. Segall, M. Yoganathan, W. Suttrop, RP. Devaty, WJ. Choyke, JA. Edmond, JA. Powell, and M. Alouani. Calculated and measured uv reflectivity of sic polytypes. *Physical Review B*, 50:10722–10726, 1994.

[15] M. Kildemo, F. Hansteen, and O. Hunderi. Details of below band-gap uniaxial dielectric function of sic polytypes studied by spectroscopic ellipsometry and polarized light transmission spectroscopy. *Journal of Applied Physics*, 91:5677–5685, 2002.

[16] P TB. Shaffer. Refractive index, dispersion, and birefringence of silicon carbide polytypes. *Applied optics*, 10:1034–1036, 1971.

[17] S. Zollner, JG. Chen, E. Duda, T. Wetteroth, SR. Wilson, and JN. Hilfiker. Dielectric functions of bulk 4h and 6h-sic and spectroscopic ellipsometry studies of thin sic films on si. *Journal of Applied Physics*, 85:8353–8361, 1999.

[18] C. Cobet, K. Wilmers, T. Wethkamp, NV. Edwards, N. Esser, and W. Richter. Optical

properties of sic investigated by spectroscopic ellipsometry from 3.5 to 10 ev. *Thin Solid Films*, 364:111–113, 2000.

[19] OPA. Lindquist, K. Järrendahl, S. Peters, JT. Zettler, C. Cobet, N. Esser, DE. Aspnes, A. Henry, and NV. Edwards. Ordinary and extraordinary dielectric functions of 4h- and 6h-sic from 3.5 to 9.0 ev. *Applied Physics Letters*, 78:2715, 2001.

[20] R. Ahuja, A F. Da Silva, C. Persson, JM. Osorio-Guillen, I. Pepe, K. Järrendahl, OPA. Lindquist, NV. Edwards, Q. Wahab, and B. Johansson. Optical properties of 4h–sic. *Journal of Applied Physics*, 91:2099–2103, 2002.

[21] C. Xie, P. Xu, F. Xu, H. Pan, and Y. Li. First-principles studies of the electronic and optical properties of 6h-sic. *Physica B: Condensed Matter*, 336:284–289, 2003.

[22] B. Adolph, K. Tenelsen, VI. Gavrilenko, and F. Bechstedt. Optical and loss spectra of sic polytypes from ab initio calculations. *Physical Review B*, 55:1422–1429, 1997.

[23] S. Ninomiya and S. Adachi. Optical constants of 6h-sic single crystals. *Japanese Journal of Applied Physics*, 33:2479–2482, 1994.

[24] M. Kildemo. Optical properties of silicon carbide polytypes below and around bandgap. *Thin solid films*, 455:187–195, 2004.

[25] F. Bechstedt, P. Käckell, A. Zywietz, K. Karch, B. Adolph, K. Tenelsen, and J. Furthmüller. Polytypism and properties of silicon carbide. *Physica Status Solidi (b)*, 202:35–62, 1997.

[26] JY. Yang, LH. Liu, and JY. Tan. First-principles molecular dynamics study on temperature-dependent dielectric function of bulk 3c and 6h-sic in the energy range 3-8ev. *Physica B: Condensed Matter*, 436:182–187, 2014.

[27] BM. Epelbaum, O. Filip, and A. Winnacker. Bulk and epitaxial growth of micropipe-free silicon carbide on basal and rhombohedral plane seeds. *Physica Status Solidi (b)*, 245:1257–1271, 2008.

[28] G. Dhanaraj, M. Dudley, RH. Ma, H. Zhang, and V. Prasad. Design and fabrication of physical vapor transport system for the growth of sic crystals. *Review of scientific instruments*, 75:2843–2847, 2004.

[29] V. Tolstoy, I. Chernyshova, and V. Skryshevsky. Handbook of infrared spectroscopy of ultrathin films, 2003.

[30] M. Shamseddine, M. Kazan, and M. Tabbal. Model for the unpolarized infrared reflectivity from uniaxial polar materials: Effects of anisotropy, free carriers, and defects. *Infrared Physics & Technology*, 55:112–121, 2012.

[31] N. Rahbany, M. Kazan, M. Tabbal, R. Tauk, J. Jabbour, J. Brault, B. Damilano, and J. Massies. Measurement of the effect of plasmon gas oscillation on the dielectric properties of p-and n-doped alxga1- xn films using infrared spectroscopy. *Journal of Applied Physics*, 114, 2013.

[32] F. Engelbrecht and R. Helbig. Effect of crystal anisotropy on the infrared reflectivity of 6h-sic. *Physical Review B*, 48:15698–15707, 1993.